Seismic and aseismic deformation in the Danakil Depression, East Africa and Corinth Rift, Greece: magma-rich vs magma-poor rift extension

Gareth L. Hurman[1], Derek Keir[1,2], Lisa C. McNeill[1], Carolina Pagli[3], Jonathan M. Bull[1] and Georgios Michas[4]

[1]School of Ocean and Earth Science, University of Southampton, Southampton, SO14 3ZH, UK

[2]Department of Earth Sciences, University of Florence, Florence, Italy

[3]Department of Earth Sciences, University of Pisa, Pisa, Italy

[4]Institute of Geodynamics, National Observatory of Athens, Athens, Greece

Abstract

The mechanisms accommodating extension in magma-rich and magma-poor rifts likely differ, with magmatic intrusion (largely aseismic) potentially dominating magma-rich rifts and faulting (seismic deformation) thought to accommodate most extension in magma-poor rifts. We compared the seismic and aseismic deformation occurring in the Danakil Depression, East Africa (magma-rich) and Corinth Rift, Greece (magma-poor) to test this hypothesis and improve understanding of extension in end-member rifts. The seismic moment release across both rifts was determined using NEIC catalogue earthquake data (from 1950-2023). In the Danakil Depression, seismic moment release is highest at the rift margins and sections of the rift axis with reduced magmatism. Seismic moment release is greatest across the eastern part of the Corinth Rift. Regional geodetic extension data were used to calculate the changing geodetic moment rates along both rifts. The ratio between the seismic and geodetic moment rates (S/G) was calculated for the entire rifts and overlapping zones along each rift. The horizontal component of the seismic moment was extracted to calculate the horizontal seismic/geodetic moment rate ratio (S_h/G). The Danakil Depression and Corinth Rift have S/G of 0.03 and 0.43, and S_h/G of 0.02 and 0.28, respectively, suggesting greater amounts of extension being accommodated by faulting in the Corinth Rift. S/G variations along the Danakil Depression are consistent with geological

indicators of along-rift variations in faulting. Relatively high S/G (~0.1) in the north of the Depression indicates that brittle deformation accommodates a significant amount of extension here, despite being potentially in the final stages of magma-rich break-up. Relatively low S/G (~0.1-0.15) in the west of the Corinth Rift supports the interpretations that aseismic deformation may be significant, potentially on a low-angle detachment at depth. This study confirms our hypothesis that in magma-poor rifts, greater amounts of extension are accommodated by seismic deformation compared with magma-rich rifts.

1. Introduction

The Danakil Depression, located in Northern Ethiopia and Eritrea (Fig. 1), and the Corinth Rift, in Central Greece (Fig. 2), are two of the fastest opening (>15 mm/yr) active continental rifts in the world (Figs. 3 and 4) (e.g., Avallone et al., 2004; Clarke et al., 1998; McClusky et al., 2010; Viltres et al., 2020), with both extensional settings associated with significant seismicity (Figs. 1, 2 and 4) (e.g., Ayele et al., 2007; Bernard et al., 2006; Illsley-Kemp et al., 2018; Jackson et al., 1982). The extensive Recent magmatism in the Danakil Depression (e.g., Keir et al., 2013; Pagli et al. 2012; Watts et al., 2020; Rime et al., 2023) means that it is defined as a magma-rich rift setting. In contrast, magmatism has been almost completely absent during the evolution of the Corinth Rift, and therefore is defined as a magma-poor rift (e.g., McNeill et al., 2019a). The western end of the active Aegean volcanic arc is located ~50 km SE of the Corinth Rift (e.g., Pe-Piper & Piper, 2005), however arc magmatism is not involved with the rifting processes across the Corinth Rift. Sitting at opposite ends of the magma-rich and magma-poor rift settings framework (e.g., Franke, 2013; Tugend et al., 2018) means that the mechanisms accommodating extensional strain in these two rift settings likely differ.

Our hypothesis is that seismic deformation (brittle faulting) contributes significantly towards extension in the magma-poor Corinth Rift (e.g., Lavier & Manatschal, 2006; Peron-Pinvidic et al., 2013; Peron-Pinvidic & Manatschal, 2009; Reston, 2009). In contrast, since the Danakil Depression is magma-rich, aseismic magmatic intrusion is hypothesised to be the dominant mechanism accommodating extension (Buck, 2006; Hayward & Ebinger, 1996). For example, over short time scales (days) of individual dyking events, seismic moment release accounts for <3% of the total extension (Belachew et al., 2011). In contrast, in areas of relatively low

magmatism in the Danakil Depression, ~30% of extension is accommodated by axial faulting over 100 k.y. time scales (Hurman et al., 2023). This study aims to better understand and compare the active deformation processes occurring in the two settings over the several decades sampled by global instrumental seismic records. As well as sitting at opposite ends of the magma-rich and magma-poor rift framework, the Danakil Depression and Corinth Rift have been selected as our comparative study regions due to both having similarly high geodetic extension rates (>15 mmm/yr) (Figs. 3 and 4) (e.g., Avallone et al., 2004; Clarke et al., 1998; McClusky et al., 2010; Viltres et al., 2020), while both being clearly definable rift segments (Figs. 1 and 3). To analyse the active deformation occurring across both rifts we calculate the geodetic moment rates from regional Global Navigation Satellite System (GNSS) data (Avallone et al., 2004; Viltres et al., 2020), as well as calculating seismic moment rates for both rifts from the Global National Earthquake Information Center (NEIC) catalogue. We will then determine the ratio between the seismic and geodetic moment rates (seismic/geodetic moment rate ratio – S/G) for the two rifts, quantifying the contribution of seismic deformation (co-seismic slip) towards releasing the time-averaged extensional strain accumulation. Geodetic moment rates represent a measure of the rate of interseismic strain accumulation across the rift, while seismic moment rates measure the co-seismic fault slip related response in the plate boundary zone.

By comparing the S/G for both the Corinth Rift and Danakil Depression, we will better understand contribution of brittle faulting towards extension in a magma-rich and magma-poor setting, and be able to compare the nature of deformation that is occurring at these two rift end-members. Furthermore, it will provide further insight into spatial variations of seismic (brittle faulting) and aseismic (e.g., magmatic intrusion, aseismic slip/creep) deformation. Previous studies comparing magma-poor and magma-rich extensional settings have typically focused on passive margins (e.g., Franke, 2013; Tugend et al., 2018), where comparative analysis of the dynamic geological deformation is not possible. Most rifts fall somewhere between the magma-rich and magma-poor rift settings end members, and/or show strong along rift variations in extension processes both temporally and spatially (e.g., Shillington et al., 2009; Sapin et al.,2021; Pérez-Gussinyé et al., 2023). Therefore, with the Danakil Depression and Corinth Rift both actively rifting and siting at opposite ends of the magma-rich and magma-poor rift framework, they are ideal study locations. Despite the

differences in extension mechanisms, there are also a number of similarities between the two rifts, such as high extension rates (e.g., Avallone et al., 2004; Clarke et al., 1998; McClusky et al., 2010; Viltres et al., 2020) and an asymmetrical rift structure (e.g., Bastow et al., 2018; Hurman et al., 2023; Nixon et al., 2016), making them good candidates for a comparative study.

Our study can also be compared with previous work that analysed geodetic and seismic moment rates for each rift. For the Corinth Rift, previous studies tended to lack detail, as they were part of regional analysis across the entirety of Greece (Chousianitis et al., 2015) or the wider eastern Mediterranean (Jenny et al., 2004; Sparacino et al., 2022; Ward, 1998) rather than specifically the Corinth Rift. Previous localised studies along the East African Rift System have compared seismic and geodetic strain rates from both local and regional catalogues, with these studies showing that short-term strain patterns can be representative of long term patterns in both magma-rich and magma-poor areas (Weinstein et al., 2017; Musila et al., 2023; Lavayssière et al., 2019; Ebinger et al., 2019). Déprez et al. (2013) also investigated the S/G along the East African Rift System, analysing the varying contribution of different deformation mechanisms and their relationship to controls such as the stage of rift evolution and thermal state of the lithosphere. However, this study only extended as far north as the Main Ethiopian Rift, thus did not include Afar and the Danakil Depression. As a result, this will be first time that analysis has been conducted for the Danakil Depression. Although previous studies from the Danakil Depression (Bastow et al., 2018; Hurman et al., 2023) have indicated along-axis variations in the mechanisms accommodating extension over the last 100 ka, this study provides the opportunity for more insight over decade long-time scales.

2. Tectonic Settings

2.1. Danakil Depression

Located in Northern Afar, the Danakil Depression is undergoing the final stages of continental break-up with the locus of extension along a series of magmatic segments (e.g., Hayward & Ebinger, 1996; Pagli et al., 2014) (Fig. 1). The Afar region is the location of the triple junction between the Red Sea, Gulf of Aden and East African Rift systems (Fig. 1) (McKenzie et al., 1970). Rifting in Afar initiated around 30 Ma and was associated with

significant plume volcanism (Hofmann et al., 1997; Wright et al., 2006; Yirgu et al., 2006). Red Sea extension initiated later at ca. 23 Ma (Szymanski et al., 2016), with extension in the southernmost part of the Red Sea rift jumping laterally on land in Northern Afar around 11 Ma, resulting in the Danakil Depression becoming the locus of extension (Eagles et al., 2002). The age of rifting is broadly consistent with the 8.5 Ma or younger age of the earliest syn-rift Red Bed sedimentary series (Brinckmann and Kürsten, 1971; Le Gall et al., 2018). The Danakil Depression extends from the Gulf of Zula in the north to the Harak Graben in the south, with the western margin bordered by the 3 km high Ethiopian Plateau, while the Danakil Block, that is 0.5-1 km in elevation, borders the eastern rift margin (Figs. 1 and 3). The thin crust beneath the Danakil Depression, 20-25 km in the south (south of 13°N) and reducing to <15 km in the north (north of 13.7°N), is indicative of the maturity of the rift and the amount of stretching that has occurred (Ahmed et al., 2022: Hammond et al., 2011; Hurman et al., 2023; Makris & Ginzburg, 1987). Crustal thickness is 40 km beneath the Ethiopian Plateau and 25-30 km beneath the Danakil Block (Ahmed et al., 2022; Hammond et al., 2011; Hurman et al., 2023). Global Navigation Satellite System (GNSS) measurements have shown that the Danakil Depression is opening by anticlockwise rotation, with the rate of extension increasing southwards, with a rate of 7 mm/yr at 15°N and increasing to ~20 mm/yr at 13°N (McClusky et al., 2010; Viltres et al., 2020) (Figs. 1b and 3).

Extension since the Quaternary in the Danakil Depression has been localised to a ~20 km wide rift axis (Wolfenden et al., 2005), with along-rift variations in extension by magmatism and faulting observed (e.g., Bastow et al., 2018; Hurman et al., 2023; Keir et al., 2015) (Fig. 1). Magmatism is most clear in the central portions of the basin, where the Erta-Ale and Tat-Ali magmatic segments are arranged in an en-echelon manner (Figs. 1a and 3), and are the location of multiple volcanic centres (e.g., Barberi & Varet et al., 1970; Keir et al., 2013) (Figs. 1a and 3) with rift-aligned diking and fissure eruptions (e.g., Moore et al., 2019; Nobile et al., 2012; Pagli et al., 2012; Watts et al., 2023). In contrast, the lateral ends of the Depression are the location of axial grabens, which host sedimentary deposits, with the axial faults having significant fault slip rates (Bastow et al., 2018; Hurman et al., 2023). For example, in the north, seismic reflection data has shown that upper crustal axial faulting accommodates significant amounts of extension (30%) over the last ~100 ka with slip rates

of up to 3.8-5 mm/yr calculated for individual faults (Bastow et al., 2018; Hurman et al. 2023).

The distribution of earthquakes from global and local catalogues shows that seismicity is primarily located along the rift axis and the western rift margin (Figs. 1 and 4a; Belachew et al., 2011; Illsley-Kemp et al., 2018). Seismicity beneath the magmatic segments is mostly limited to M <3.5 microseismicity observed only by local seismic networks (Figs. 1 and 4a; Belachew et al., 2011; Illsley-Kemp et al., 2018), whereas larger earthquakes (M >4) occur at the rift ends and along the western rift margin (Figs. 1 and 4a; Belachew et al., 2011; Illsley-Kemp et al., 2018; La Rosa et al., 2021a). For example, InSAR analysis to the north of the Dallol region has shown significant fault slip and accompanying large earthquakes (M_w >5) have occurred in the absence of magmatic intrusion (La Rosa et al., 2023). Significant large magnitude earthquakes have occurred away from the rift axis, including along the western rift margin (Fig. 1) (Ayele et al., 2007; Illsley-Kemp et al., 2018; Zwaan et al., 2020b; La Rosa et al., 2021b), where a M_w 5.6 event occurred as part of an earthquake swarm in 2002 near the town of Mekele (Ayele et al., 2007).

2.2. Corinth Rift

Located in Central Greece, the Corinth Rift is a narrow rift (~40 by 100 km) undergoing N-S orientated extension (Figs. 2 and 4). The rift started forming ~4-5 Ma, cutting across the N-S Hellenide Orogen in the western part of the rift (Bell et al., 2018; Gawthorpe et al., 2017). Various mechanisms have been suggested for the rift's formation, including gravitational collapse of overthickened crust (e.g., Le Pourhiet et al., 2003), extension due to rollback of the subducting African plate occurring along the Hellenic Trench (Fig. 4) (e.g., Doutsos et al., 1988; Jolivet et al., 1994) and propagation of the dextral North Anatolian Fault (Fig. 4) to the SW (e.g., Armijo et al., 1996; 1999). Evolution of the Corinth Rift occurred in three main phases of development, with the first phase occurring 5-3.6 to ~2.5-2 Ma. During this period the Corinth Rift was south of its current location, with a 20-30 km wide zone of deformation that extended as far north as the current southern margin of the Gulf of Corinth (Figs. 2 and 4) (Gawthorpe et al., 2017). The second phase of rift evolution occurred ~2.5-2 to 0.8 Ma, with northward migration to the current location of the Corinth Rift (Figs. 2 and 4). Phase 3 represents the ~0.8 Ma to present and was marked by a further

northward migration of deformation (McNeill et al., 2019b), development of the border fault system, progressive fault linkage and an acceleration in fault slip rates (Nixon et al., 2016; 2024).

The Corinth Rift has been almost completely amagmatic during its evolution (e.g., McNeill et al., 2019a), with extension now focused along a network of major N-dipping faults that straddle the southern margin of the Gulf of Corinth in an en-echelon arrangement (Fig. 4). These faults, which range from 10-25 km in length, have become progressively linked over the last 340 kyr and are now kinematically coherent and linked at depth, forming a fault network totalling 130 km in length (e.g., Bell et al., 2009; Nixon et al, 2016; 2024). Significant slip has occurred along the southern margin border faults, with estimated Quaternary slip rates reaching ~3-7 mm/yr for the faults along the southern margin (e.g., Armijo et al., 1996; Bell et al., 2009; De Martini et al., 2004; McNeill & Collier, 2004; McNeill et al., 2005; Nixon et al., 2024), and increasing during the Holocene (e.g., Pirazzoli et al., 2004; Stewart, 1996; Stewart & Vita-Finzi, 1996). The current extensional regime in the Corinth Rift shows an increase in extension rate from <5 mm/year in the east to up ~20 mm/year in the west of the rift (Figs. 2 and 4) (e.g., Avallone et al., 2004; Clarke et al., 1997; McClusky et al., 2000). In contrast, the highest extension rates on geological time scales are in the central rift, as indicated by long-term deformation patterns and whole-crust extension estimates (Bell et al., 2009; 2011; Nixon et al., 2016; 2024).

High extension and fault slip rates in the Corinth Rift have resulted in significant seismicity across the rift, including events with a M_w >6 (e.g., Bernard et al., 1997; Jackson et al., 1982) (Figs. 2 and 4). The western end of the Corinth Rift is the most seismically active region (Figs. 2, 4 and 5c), with intense microseismicity and seismic swarms (e.g., Bernard et al., 2006; Duverger et al., 2015; 2018; Kaviris et al., 2017; 2021; Papadimitrou et al., 2022), such as the 2013 Eliki (e.g., Kapetanidis et al., 2015; Mesimeri et al., 2016) and the 2015 Malamata (De Barros et al., 2020) swarms. The seismicity in the western end of the Corinth Rift has been hypothesised to relate to a postulated low-angle north-dipping layer beneath the gulf (e.g., Duverger et al. 2018; Kapetanidis et al. 2021; Kaviris et al., 2021; Lambotte et al. 2014). Larger events have also been recorded at the western end of the rift, such as the 1995 Aigion earthquake (M_w 6.2) (Bernard et al., 1997) (Fig. 4). Although sparser than the west, significant seismicity is also occurring in the eastern Corinth Rift (Figs. 2; 4 and 5c), including

the largest earthquake sequence of recent times which occurred in 1981 around the Alkyonides Gulf with the 3 main events ranging from *M* 6.3-6.7 (e.g., Jackson et al., 1982) (Fig. 4). In 2020, there was an earthquake sequence around the Perachora Peninsula at the eastern end of the Corinth Rift, with the largest event being a M_w 3.9 earthquake (Michas et al., 2022). Despite Quaternary fault slip rates being highest in the central region of the Corinth Rift (Bell et al., 2009; Nixon et al., 2024), this part of the rift has reduced seismic activity relative to the eastern and western ends of the rift, although there have still been major earthquakes such as the 1992 Galaxidi earthquake (*Ms* 5.9) on the northern margin of the rift (Hatzfeld et al., 1996) (Fig. 4).

3. Data and Methods

3.1. Quantifying Geodetic Moment Rates

To calculate the variation in geodetic strain along the Danakil Depression and Corinth Rift, we used the GNSS velocity data from the two extensional settings (Avallone et al., 2004; Viltres et al., 2020) (Figs. 1b and 2b). The study area for the Danakil Depression is defined as from the Gulf of Zula in the north to the Harak Graben in the south, a length of 360 km (Fig. 1). The width of the study area is 180 km, encompassing the western margin border fault system, and stepping eastwards in the south to include the Nabro Volcanic Complex (NVC) (Fig. 1). The Corinth Rift study area has the same 2:1 ratio of length to width, with the study area extending from west of the Trizonia Basin to east of the Alkyonides Gulf, a distance of 145 km and a width of 72.5 km (Figs. 2 and 4).

Extensional velocities have then been resampled at equal distances along the rift to enable calculation of the geodetic moment rate for a series of overlapping rectangular zones. These zones have equal aspect ratios of 4.5:1 for both rift settings, for the Danakil Depression they are 180 km (l) wide and 40 km (L) in length (overlap of 20 km), and for the Corinth Rift they have the same relative dimensions of 72.5 km (l) wide and 16.1 km (L) in length (overlap of 8.05 km). It is assumed that the direction and magnitude of the extensional velocity have remained constant over the duration of the observational period. The geodetic strain rate (ϵ) is quantified as the ratio between the velocity (v) and the box width (l).

$$\epsilon = v / l \qquad (1)$$

Then the geodetic moment rate is determined using the definition of the strain tensor rate as outlined by Kostrov (1974).

$$2\,\mu\,A\,Hs\,\epsilon = M_{geodetic} \qquad (2)$$

Using μ the shear modulus as 3×10^{10} N m^{-2} (typical shear modulus value for the crust) for both the Danakil Depression and Corinth Rift, $A = l \times L$ the surface area of each study zone and *Hs* the seismogenic thickness.

To define the seismogenic thickness (*Hs*) of each rift we used local seismic catalogues (Fig. 5). For the Danakil Depression we used a catalogue of earthquakes compiled from Belachew et al. (2011) and Illsley-Kemp et al. (2018) that occurred between 2007-2013, with events with an error >5 km in latitude, longitude and/or depth location removed. We have defined the seismogenic (*Hs*) thickness as the depth above which 90% of events have occurred. Previous seismic-geodetic moment rate studies have also used a 90% cut-off point to define the seismogenic thickness (e.g., Pancha et al., 2006; Sparacino et al., 2022). Applying this criterion results in the seismogenic thickness (*Hs*) being identified as 15 km (Fig. 5b), with 10% of events occurring below this depth. The local catalogue used for the Corinth Rift was taken from the Hellenic Unified Seismic Network (HUSN), consisting of events recorded between 2012-2023. The earthquakes show a different depth pattern compared with the Danakil Depression catalogue, with fewer shallow (<5 km) events and the majority of earthquakes occurring between 7-15 km depth (Fig. 5d). Using the local seismicity catalogue, we have defined the seismogenic thickness (*Hs*) for the Corinth Rift as 19 km depth with 90% of earthquakes occurring above this depth (Fig. 5d).

3.2. Danakil Depression Geodetic Data

The geodetic moment rate was calculated using GNSS data from Viltres et al. (2020), collected between 2001-2016 (Fig. 1). The survey sites used for this study were along the length of the Eritrean coastline, from the Gulf of Zula down to the Gulf of Tadjoura (Djibouti) southwards (Fig. 1b). Therefore, we have geodetic extension rate data for the entire length of the Danakil Depression. The extension rates are relative to a stable Nubia plate, and representative of the full extensional velocity of the Danakil plate relative to the Nubian plate due to the distance between the survey sites and the rift axis (Fig. 1b).

3.3. Corinth Rift Geodetic Data

For the Corinth Rift, GNSS derived extension rates from Avallone et al. (2004) have been used, with the velocity data collected between 1990-2001 (Fig. 2b). Although, there have been numerous geodetic studies across the Corinth Rift, this study was favoured due to the density of GNSS sites along the margins of the Corinth Rift, whilst also having a longer observational period than other studies (e.g., Briole et al., 2000). The calculated rates for the Corinth Rift used for this study are relative to the Peloponnese (Fig. 2b). Despite the density of sites, the number is reduced at the eastern end of the Corinth Rift study area (Fig. 2b), and we therefore have interpolated the extension rate for this area of the rift when calculating the geodetic moment rate. The interpolated extension rates for the eastern end of the rift are <5 mm/yr, which is in agreement with other geodetic studies that have a denser network of GNSS sites in the east (e.g., Clarke et al., 1998).

3.4. Earthquake Data and Quantifying the Seismic Moment Release and Rate

To calculate the seismic moment release and rate of each setting, we have compiled the National Earthquake Information Center (NEIC) earthquake catalogues for both the Danakil Depression and Corinth Rift (Figs. 1 and 2). The earthquake data was not declustered to remove aftershocks or swarms associated with dike intrusions because we assume that stress release from aftershocks is much smaller than the main shock. We also assume that earthquakes are a consequence of long-term plate boundary stress accumulation, and that the magmatic cycle is a minor contribution. Further processing of the NEIC catalogue data for the two rifts was conducted to improve the comparability and quality of the data. Earthquake events that occurred prior to 1950 were removed, with both catalogues showing a significant degree of incompleteness prior to this date (particularly for the Danakil Depression). Additionally, having the seismicity data of the two rift settings covering the same time period (73 years) allows more comparable seismic moment rates to be calculated. We also removed earthquakes that occurred at a deeper depth than the maximum crustal thickness for each of the rifts. This was particularly important for the Corinth Rift due to the close proximity of the Hellenic Trench subduction zone and underlying plate (Fig. 4), with seismicity at a deeper depth related to plate subduction rather than extension of the upper plate. The Ethiopian Plateau has the thickest crust in the

Danakil Depression study area (Ahmed et al., 2022: Hammond et al., 2011; Hurman et al., 2023), so a cut off depth of 40 km was used to filter the seismicity data. In the Corinth Rift, the deepest Moho depth is ~40 km at the western end of the rift (e.g., Sachpazi et al., 2007; Tiberi et al., 2001) therefore the same cut off point of 40 km was used for the Corinth Rift data. The average epicentre location errors quoted for the filtered NEIC catalogues used for this study are 9.2 km for the Danakil Depression and 4.9 km for the Corinth Rift (https://earthquake.usgs.gov/). Studies in East Africa, however, have compared locations from local networks with NEIC catalogues and found mislocations of up to 25 km (Weinstein et al., 2017).

Calculation of the seismic moment release also requires body wave magnitudes (mb) in the NEIC catalogue to first be converted to moment magnitudes (M_w). To do this we used the linear relationship defined by Scordilis (2006) using the conversion equation (3)

$$M_w = 0.85\ (+/-\ 0.04)mb + 1.03\ (+/-\ 0.23) \quad (3)$$

We assessed the magnitude of completeness (*Mc*) of the NEIC data by producing Gutenberg-Richter plots for both regions (Figs. 1c and 2c). *Mc* is 4.5 for the Danakil Depression and 4.2 for the Corinth Rift, likely due to the denser seismic station distribution in Europe compared to Africa.

We converted our moment magnitude (M_w) values to seismic moment release (M_0). Kanamori (1977) defined the relationship between seismic moment magnitude (M_w) and seismic moment release (M_0) using equation (4)

$$M_w = 2/3 \log_{10} (M_0) - 10.7 \quad (4)$$

To convert our M_w values to M_0 we rearranged equation (4) to equation (5)

$$M_0 = 10^{1.5(Mw + 10.7)} \quad (5)$$

The seismic moment release values were then divided by 10^7 to convert the values from dyne-cm to newton meters (Nm).

To help represent the spatial variation in seismic moment release across both the Danakil Depression and Corinth Rift, we summed the seismic moment release in grid cells with dimensions of 20 x 20 km (Figs. 6 and 7). To calculate the seismic moment rate we

normalized the seismic moment release values by 73, the number of years (1950-2023) that the filtered NEIC catalogues for each of the rifts cover.

We also used the Gutenberg-Richter relation to evaluate the seismic moment release that is missing below the cut off magnitude down to a magnitude of 0. To do this we calculated b-values of the seismic catalogue (1.1 for Danakil Depression and 1 for the Corinth Rift), from which we modelled the magnitude frequency distribution, and resultant seismic moment release that we did not record below the cut-off magnitude. The results show that we under-sample the seismic moment release by 35% for the Danakil Depression, and 10% for the Corinth Rift.

3.5. Seismic/Geodetic Moment Rate Ratio

To constrain the contribution of seismic deformation towards extension across both the Danakil Depression and Corinth Rift, we calculate the ratio between the cumulative seismic moment rate and the geodetic moment rate, which is the seismic/geodetic moment rate ratio (S/G). For calculating S/G for each of the rifts, we used the total seismic moment rate for the entire study area and a geodetic moment rate value derived from the mean geodetic extension rate of the rift (Table 1). To understand spatial variations, we calculated the S/G in overlapping zones along rift using the total seismic moment rate of each of the zones and the geodetic moment rate calculated for the same zone (Figs. 8; 9; Table 2 and 3). The calculation therefore takes into account the varying extension rates along both rifts.

3.6. Horizontal Seismic/Geodetic Moment Rate Ratio

The geodetic moment rate represents the total crustal deformation occurring in a horizontal direction over the time period of observations, therefore extracting the horizontal component of the seismic moment rate improves the comparability of the moment rate types when calculating S/G. To calculate the horizontal component of the seismic moment rate we corrected for the dip of the faults along which the seismic deformation occurs. We assumed a fault dip range of 40-60°, typical for seismogenic normal faults (e.g., Anderson, 1951), to calculate the horizontal component of the seismic moment rate. Although many individual faults dips are resolved in both rift systems, there is some debate over fault dips at depths, hence we chose to use this global dip range, with the median horizontal

component of the seismic moment rate calculated using a 50° fault dip. We then determined the ratio between the extracted horizontal component of the seismic moment rate and the geodetic moment rate (S_h/G) for the entire Danakil Depression and Corinth Rift (Table 1), as well as for overlapping zones along the rifts (Figs. 8; 9; Tables 2 and 3).

4. Results

4.1. Danakil Depression

4.1.1. Danakil Depression Seismic Moment Release

The 20 x 20 km grid of total summed seismic moment release across the Danakil Depression highlights significant variation in the rift over the last 73 years. The total calculated seismic release across the Danakil Depression study area was 8.9 x 10^{18} Nm, with maxima located off-axis for the Nabro Volcanic Complex (NVC) situated in the centre of the Danakil Block, and along the western Afar margin (Fig. 6). In the north of the Depression, clusters of seismicity have resulted in elevated summed seismic moment values along or close to the rift axis, for example in the Dallol area and to the west of the Gulf of Zula. However, elsewhere along the rift axis the summed seismic moment values are low, including along the Erta-Ale and Tat-Ali magmatic segments in the central and southern part of the Danakil Depression (Fig. 6). Other large sections of the rift axis in the central and southern parts of the Danakil Depression appear to have no seismic activity (M_w >3.5) at all (Figs. 1 and 6). The results highlight how seismicity in the north of the Depression is focused along or close to the rift axis (Fig. 6), whereas in the centre and southern part of the Depression, seismic moment values are greater at the sides of the rift, such as along the western marginal graben system and the NVC but reduced along the axial magmatic segments (Fig. 6).

4.1.2. Danakil Depression S/G and S_h/G

The seismic moment rate for the entire Danakil Depression ranges from 3.27 x 10^{16} – 4.60 x 10^{17} Nm/yr and has a median rate of 1.10 x 10^{17} Nm/yr (Table 1). Using the mean geodetic extension rate of 13 mm/yr, a geodetic moment rate value of 4.23 x 10^{18} Nm/yr was calculated (Table 1). Therefore, the S/G ratio for the entire Danakil Depression study area is 0.03. The horizontal seismic moment rate for the entire Danakil Depression ranges from 2.24 x 10^{16} Nm/yr to 3.62 x 10^{17} Nm/yr, with a median rate of 7.85 x 10^{16} (50° fault dip)

(Table 1). With a geodetic moment rate of 4.23 x 10^{18} Nm/yr for the Danakil Depression, the median S_h/G ratio for the entire rift is calculated as 0.02 (Table 1). The seismic and geodetic moment rates were also calculated for 16 Zones with dimensions of 180 km across axis and 40 km along axis (20 km overlap) (Fig. 8a; Table 2), to provide measures of spatial variability in S/G and S_h/G. In the Danakil Depression, the geodetic moment rate increases from north to the south (Fig. 8b; Table 2) due to the southward increase in extension rates (Fig. 1) (up to 20 mm/yr) (McClusky et al., 2010; Viltres et al., 2020). The geodetic moment rate is ~1.35 x 10^{17} Nm/yr at 20 km (Zone 1) in the north, and progressively increases to a maximum value of ~7.1 x 10^{17} Nm/yr at 340 km (Zone 16) in the south (Fig. 8b; Table 2). The seismic moment rate along the rift axis of the Danakil Depression however shows more variability (Fig. 8c; Table 2). The highest seismic moment rates occur at 100-120 km (Zones 5-6) and at 300 km (Zone 14) reaching median values of up to ~3.3 x 10^{16} Nm/yr, caused by the significant seismicity across the Dallol area and the NVC (Figs. 1; 8c and Table 2). Other sections of the rift axis show minor peaks (1.2-2.2 x 10^{16} Nm/yr) in seismic moment rate at 20-40 km (Zone 1-2), 180-200 km (Zone 9-10) and 240 km (Zone 12) along the rift axis, which coincide with the seismicity that has occurred west of the Gulf of Zula, the western margin graben system and NVC, respectively (Figs. 1; 7c and Table 2). The lowest seismic moment rates (~1.1-1.4 x 10^{15} Nm/yr) are at 60-80 km (Zone 3-4) and 340 km (Zone 16) (Fig. 8c and Table 2).

The S/G value does not go above 0.1 for any of the zones in the Danakil Depression (Fig. 8d and Table 2). The maximum S/G value of 0.095 occurs at 20 km (Zone 1) and 100-120 km (Zone 5-6) (Fig. 8 and Table 2), where the Gulf of Zula and Dallol region are located (Fig. 1). There are minor peaks in S/G that coincide with the increased seismic moment rates observed off axis, with a S/G value of ~0.045 at 180-200 km (Zones 9-10) (Fig. 8 and Table 2), where the western margin graben system is located (Fig. 1). For the NVC (Fig. 1) at 260-340 km (Zones 13-16), the S/G reaches a maximum value of ~0.05 (Fig. 8 and Table 2). Despite the highest median seismic moment rate value (~3.3 x 10^{16} Nm/yr) being at the southern end of the Danakil Depression (260-340 km), the high extension rates (~20 mm/yr) in this area result in an S/G value half that observed in the Dallol area despite having similar seismic moment rates (Fig. 8 and Table 2).

Despite being lower in value, the horizontal seismic moment rates have the same along axis variation as the total seismic moment rates (Table 2). Therefore, the along axis S_h/G ratio values are lower than the S/G but show the same overall along axis pattern (Fig. 8). With the highest S_h/G ratios calculated along the Danakil Depression at 20 km (Zone 1) and 100-120 km (Zone 5-6), with median ratio values reaching ~0.06 (Fig. 8f; Table 2). There are minor peaks of ~0.03 S_h/G at 180 km (Zone 9) and 300 km (Zone 14), with the ratio remaining ≤~0.02 for the remaining zones of the Danakil Depression (Fig. 8f; Table 2).

4.2. Corinth Rift

4.2.1. Corinth Rift Seismic Moment Release

The total seismic moment release for the Corinth Rift is 5.2 x 10^{19} Nm. The summed seismic moment release for 20 x 20 km cells in the Corinth Rift shows increased values across the northern margin of the Gulf of Corinth compared with the southern margin (Fig. 7). The east of the Corinth Rift in particular shows elevated seismic moment release (around the Alkonyides Gulf), mainly due to the 3 large earthquakes (*M* 6.3-6.7) in 1981 (Fig. 4) (e.g., Jackson et al., 1982). Elevated summed seismic moment release is also observed to the northeast of the Trizonia Basin (Fig. 7), caused by the *Ms* 6.2 1995 Aigion Earthquake and related aftershocks (Fig. 4) (e.g., Bernard et al., 1997). The southern rift margin may have apparent low seismic moment release (Fig. 7), but this is partly a result of the seismicity associated with the N-dipping border fault system of the southern margin occurring at depth and thus being located beneath the Gulf or its northern margin. Other significant earthquake events along the northern margin, such as the 1992 Galaxidi earthquake (*Ms* = 5.9) (Hatzfeld et al., 1996), have also contributed to elevated seismic moment release (Fig. 7). The most intense seismicity in the Corinth Rift occurs at its western end (Figs. 2 and 4), however the seismic moment release is relatively low (Fig. 7) due to the typically lower magnitudes of these events (Figs. 2 and 4).

4.2.2. Corinth Rift S/G and S_h/G

Seismic moment rates for the entire Corinth Rift range from 2.93 x 10^{17} – 2.86 x 10^{18} Nm/yr, and have a median value of 7.12 x 10^{17} Nm/yr (Table 1). The geodetic moment rate for the entire rift is 1.65 x 10^{18} Nm/yr, derived from the mean geodetic extension rate of 10 mm/yr

(Table 1). Therefore, an S/G value of 0.43 was calculated for the entire Corinth Rift (Table 1). The horizontal seismic moment rate ranges from 1.46 x 10^{17} – 2.19 x 10^{18} Nm/yr, with a median value of 4.58 x 10^{17} Nm/yr (50º fault dip) (Table 1). With a geodetic moment rate of 1.65 x 10^{18} Nm/yr for the Corinth Rift, the median S_h/G ratio for the entire rift is calculated as 0.28 (Table 1). Seismic and geodetic moment rates were also calculated for 17 zones with dimensions of 72.5 km across axis and 16.1 km along axis (8.05 km overlap) (Fig. 9 and Table 3), which is the same ratio of width to length as the 180 x 40 km zones of the Danakil Depression. The geodetic rate in the Corinth Rift increases from the east to west because of the increasing extension rates, from <5 to 17 mm/yr (e.g., Avallone et al., 2004) (Figs. 2 and 9b, Table 3). At the western end of the Corinth Rift, the maximum geodetic moment rate is 3.27 x 10^{17} Nm/yr (Zone 1), which decreases to a value of 7.65 x 10^{16} Nm/yr at the eastern end of the rift (Zone 17) (Fig. 9b and Table 3). In the western and central parts of the Corinth Rift (~0-100 km; Zones 1-12) the median seismic moment rate does not exceed 6 x 10^{16} Nm/yr (Fig. 9c). An exception is Zones 6 and 7 (~40-60 km) in the centre of the rift, with a slightly elevated median seismic moment rate (~1.0 x 10^{17} Nm/yr) (Fig. 9c and Table 3) due to the 1995 Aigion earthquake (Fig. 4). The highest seismic moment rates occur at the eastern end of the Corinth Rift, with median values reaching ~1.9 x 10^{17} Nm/yr for Zones 13-14 (~105-115 km) and Zone 17 (~135 km) (Fig. 9c and Table 3), as result of the 1981 earthquakes (Fig. 4).

The S/G along the Corinth Rift shows significant variation, with a ratio of ~0.1-0.15 in the west (Zones 1-5; 0-40 km) increasing to ~0.4 in the centre (Zones 5-11; 40-100 km), and is >1 for a number of zones (13-14, 16-17) in the east, with maximum S/G of ~2.2-2.4 for Zones 13-14 and 17 (~105-115, ~135 km) (Fig. 9d and Table 3). The horizontal seismic moment rates show the same along axis variation as the total seismic rates despite being lower in value (Table 3). Therefore, the along axis S_h/G ratio values in the Corinth Rift are lower than the S/G but show the same the along axis pattern (Fig. 9). S_h/G ratios for the western end of the Corinth Rift (Zones 1-5; 0-40 km) are ≤~0.1, and the centre of the rift (Zones 5-11; 40-100 km) ranging from ~0.15-0.3 (Fig. 9e; Table 3). Despite using the horizontal component of the seismic moment rate to calculate S_h/G (reducing the seismic moment rate), the ratio is still >1 for zones 13-14 and 17 (~105-115, ~135 km) with values of ~1.4-1.6 (Fig. 9e; Table 3).

5. Discussion

Calculating the ratio between seismic moment rate and geodetic moment rate (S/G) across both the Danakil Depression and Corinth Rift has produced values of 0.03 and 0.43, respectively (Table 1). With a horizontal seismic/geodetic moment rate ratio (S_h/G) of 0.02 for the Danakil Depression, and 0.28 for the Corinth Rift (Table 1). This shows that significantly greater amounts of seismic deformation occur in the magma-poor Corinth Rift compared with the magma-rich Danakil Depression. This suggests that brittle faulting is accommodating more extension in the Corinth Rift, whereas in the Danakil Depression aseismic deformation (such as magmatic extension) dominates, as might be expected. However, extrapolating the use of relatively short earthquake catalogues to understand rift behaviour over geological significant time periods requires careful consideration of the time and length scales of the observations. The ~70-year period of the seismic catalogues is shorter than the seismic cycle of the faults in the rifts. For example, recurrence intervals of the order of ~200-600 years have been calculated for Corinth Rift border faults from paleoseismological fault trenching (e.g., Collier et al., 1998; Koukouvelas et al., 2001; McNeill et al., 2005; Pantosti et al., 2003), and therefore the catalogue may be under or over sampling the co-seismic slip compared to the long-term average patterns. However, given the length of our catalogue and that the scale of each study area includes a large number of individual faults / fault segments, it is reasonable to interpret the rift scale S/G values with some degree of confidence. S/G values for the individual zones within the rifts, which approach the length scale of single faults, should however be considered with more caution.

A major factor that must also be considered when calculating the S/G of the rifts is the seismogenic thickness value (*Hs*) used. We tested the sensitivity of the S/G regarding this parameter by applying a seismogenic thickness defined by the shallowest 70% of the seismicity (instead of 90%). This resulted in a seismogenic thickness of 6 km for the Danakil Depression and 13 km for the Corinth Rift. With these alternative seismogenic thickness values, the S/G increases to 0.07 and 0.63 for the Danakil Depression and Corinth Rift, respectively. Therefore, the same pattern of a higher S/G in the magma-poor rift Corinth Rift is still observed, with a greater proportion of seismic deformation accommodating

extension. However, it does highlight the importance of having an accurately constrained seismogenic depth, as it can impact the S/G ratio.

In this discussion section we mostly refer to S/G values rather than the S_h/G, to allow comparison with previous seismic/geodetic studies in both East Africa and Greece, as well as other rift settings, which have not extracted the horizontal component of the seismic moment rates. While the same spatial variations in S/G along axis for both the Danakil Depression and Corinth Rift are observed in the S_h/G values, although lower in value.

5.1. Danakil Depression

Variations in the observed S/G correlate well with the changes in extensional style that occur along the along the length of the Danakil Depression (e.g., Bastow et al., 2018; Hurman et al., 2023; La Rosa et al., 2023). The maximum S/G ratio values of ~0.1 (~0.06 S_h/G) are observed at the northern end of the Depression (Zones 1, 5 and 6) (Fig. 8 and Table 2), suggesting this is the part of the rift with the highest contribution of seismic deformation (brittle faulting) towards extension. Sections of the Danakil Depression with reduced S/G (<0.04) coincide with the location of axial volcanic centres and magmatic segments (Fig. 7), indicating that magmatic intrusion accommodates a significant amount of extension along these parts of the rift axis. Minor increases in S/G (~0.04-0.05) in the central and southern parts are related to off-axis seismic deformation (e.g., western marginal faults and the NVC) (Figs. 1, 5 and 7), indicating that border fault seismicity, and triggered seismicity from magmatism contribute little to total extension.

Previous studies have also identified the importance of crustal faulting in the northern part of the Danakil Depression (e.g., Bastow et al., 2018; Hurman et al., 2023), including InSAR observations which show evidence for tectonically-driven fault slip (La Rosa et al., 2023). In the Dallol area of Northern Afar, it has been calculated that axial faulting has accommodated ~30% of extension in the last ~100 kyr (Hurman et al., 2023). This study indicates that in the shorter-term (last ~70 years) at least ~10% (S/G = ~0.1) of the geodetic extension is accommodated by seismic deformation (Fig. 8 and Table 2).

Other than the issues considered at the start of the discussion relating to the use of an earthquake catalogue with length shorter than the seismic cycle, the seismogenic thickness value may be the potential reason for the discrepancy between short and longer term

measurement of the contribution to extension from faulting. Estimates for the effective elastic plate thickness in the Danakil Depression from modelling gravity and topography data gives *Te* of ~6 km (Hayward & Ebinger, 1996), lower than the 15 km thickness used in this study based on seismicity depths (Fig. 5). This means that 10% extension being accommodated by seismic deformation in the north of the Danakil Depression is potentially an underestimation, since using a thinner elastic layer will yield lower geodetic moment rates. Using the lower elastic thickness (6 km) yields an S/G value for the Dallol area (Zone 6) of 0.23 which better matches the 30% longer term contribution from faulting.

5.2. Corinth Rift

The Corinth Rift is an area of high seismic activity with a number of large faults accommodating extension across a narrow deformation zone. Therefore, the low S/G values of <0.5 (<0.3 S_h/G) in the western and central regions (Zones 1-12) of the Corinth Rift are surprising (Fig. 9 and Table 3), with seismic deformation expected to be the dominant mechanism accommodating extension. Chousianitis et al. (2015) also observed this discrepancy between the seismic moment and geodetic moment rates for the western versus the eastern region of the Corinth Rift. Their study divided the rift into eastern and western study areas, with the western area equivalent to our Zones 1-7, and eastern area equivalent to our Zones 7-16 (Fig. 9) (cutting off Zone 17), with geodetic to seismic moment rate ratios (G/S) of 3.19 (equivalent S/G value is 0.31) for the west and 2.48 (equivalent S/G value is 0.4) for the east respectively (Chousianitis et al., 2015). Their eastern study area does not include all 3 of the main 1981 earthquakes that occurred around the Alkyonides Gulf (Chousianitis et al., 2015) (Fig. 4), which is the likely reason, alongside the lower geodetic rates here, for the large discrepancy between the seismic and geodetic moment rates in the east. The low S/G ratio we observe at the western end of the rift does appear to be an accurate representation of the deformation pattern however, as a similar S/G ratio was calculated for both studies despite Chousianitis et al. (2015) using a more localised seismic catalogue (SHARE European Earthquake Catalogue) and a different seismogenic thickness (15 km). The significant microseismicity in the western Corinth Rift (e.g., Duverger et al. 2018; Lambotte et al., 2014; Papadimitrou et al., 2022), which is not included in our catalogue due to them being below the cut-off magnitude, can only account for ~10% of the discrepancy between the seismic moment and geodetic moment rates, thus there would

still be a shortfall in the amount of extension. Therefore, there is also likely a significant contribution from aseismic deformation to explain the S/G values observed, perhaps due to long-term aseismic deformation or creep. This aseismic deformation or creep could occur along a low angle detachment which has been proposed at depth in the western rift (e.g., Bernard et al., 2006; Chousianitis et al., 2015; Duverger et al., 2018), although the presence of this structure is debated (e.g., Bell et al., 2018) and may be immature (Lambotte et al., 2014). Regional studies across the eastern Mediterranean have also calculated an intermediate (0.25-0.5) S/G ratio for the Corinth Rift (e.g., Sparacino et al. 2022) aligning with our 0.43 S/G across the overall rift (Table 1), further supporting a significant component of aseismic deformation occurring or catalogue incompleteness. In summary, the S/G values of the magma-poor Corinth Rift are still higher than those calculated for the magma-rich Danakil Depression, in spite of components of aseismic deformation, and appear to be representative of the style of deformation.

5.3. Magma-Rich vs Magma-Poor Rift Deformation

The Corinth Rift has consistently higher S/G values than the Danakil Depression (Figs. 8; 9; Tables 2 and 3). This is consistent with the magma-poor nature of the Corinth Rift, with seismic deformation associated with brittle faulting dominating extension. For the Danakil Depression, the majority of deformation is aseismic in nature with magmatism interpreted to accommodate the majority of extension along axial magmatic segments. Although, the Corinth Rift has a far higher S/G than the Danakil Depression (Table 1), the S/G of the northern Danakil Depression and the western area of the Corinth Rift (~0.1-0.15) are similar (Figs. 8, 9; Tables 2 and 3), highlighting that brittle faulting is significant in parts of the Danakil Depression and that locally, faulting potentially accommodates a similar proportion of deformation in limited parts of the two rifts.

The comparative ages of the Danakil Depression and Corinth Rift, as well as their current stages of rift evolution, should be considered when discussing their differences in the contribution of seismic and aseismic mechanisms to extension. Rifting in the Danakil Depression is thought to have initiated ~11 Ma as suggested by plate kinematic models of the Danakil Block rotation (Eagles et al., 2002; McClusky et al., 2010). This age is broadly consistent with the <8.5 Ma age of the syn-rift Red Bed sedimentary series, indicative of rift

related subsidence (Brinckmann and Kürsten, 1971; Le Gall et al., 2018). The Corinth Rift started forming ~4-5 Ma (Bell et al., 2018; Gawthorpe et al., 2017), and therefore the two rifts are not drastically dissimilar in age. We do not therefore interpret rift age to be a primary control on the differences in rifting style in the Danakil Depression and Corinth. Instead, the thermal state of the mantle (hot beneath Afar and normal beneath Corinth) likely results in magma-rich and magma-poor extension throughout their respective rift histories.

The two rifts show slight differences in earthquake distributions with depth. The majority of earthquakes in the Danakil Depression occur in the upper 15 km (Fig. 5a-b), whereas in the Corinth Rift the majority of events occur above ~20 km (Fig. 5c-d). This corresponds to the differences in upper crustal thickness and thermal structure in each rift, with thinner crust and higher heat flow due to increased thinning and the presence of magmatism in Danakil, resulting in thinner elastic plate thickness. Seismic and geodetic moment rates have been calculated south of Afar along other segments of the East African Rift System (EARS), with variations in S/G linked to the thermal structure of the lithosphere associated with the different stages of rift evolution (Déprez et al., 2013). Higher S/G values are calculated for the more immature rift segments towards the southern end of the EARS, such as the Western (~0.6-1.25) and Eastern (~0.1-0.35) branches of the Tanzanian Craton and the Malawi Rift (~0.1-0.25) (Déprez et al., 2013). Whereas, further north along the more mature Main Ethiopian Rift (MER), the S/G decreases to ≤0.04, attributed to increased magmatism (Déprez et al., 2013). The S/G we calculate for the Danakil Depression is similar to that of the MER (0.03) despite the differences in extension rate. These low S/G values therefore potentially represent typical values for magma-rich end member rifts.

Sawires et al. (2021) analysed the S/G across Egypt, including the northern Red Sea Rift, which is undergoing the final stages of continental break-up, with full seafloor spreading occurring in the southern Red Sea (e.g., Ehrhardt & Hübscher, 2015). The S/G for the northern Red Sea are <0.04 (Sawires et al., 2021), the same as the Danakil Depression (0.03) (Table 1), suggesting the two settings are at similar stages in maturity with dominantly aseismic extension occurring, likely through magmatic intrusion.

Other studies investigating the coupling between seismic and geodetic moment rates in extensional settings have also identified significant variations in S/G, implying the relative

627 contribution of seismic deformation towards extension can vary within a single rift setting.
628 For example, across the Southern Apennines, calculated S/G values vary considerably from
629 <0.2 to >0.8 (Palano et al., 2011).

630 Overall, our study directly demonstrates that seismic deformation contributes more to
631 extension at magma-poor rifts, compared with magma-rich rifts, with aseismic magmatic
632 intrusion likely accommodating the majority of extension in late-stage magma-rich rifts.
633 However, even in extensional settings where magma is absent, a significant proportion of
634 extension may still be aseismic.

635 ## 6. Conclusions

636 We calculated the seismic and geodetic seismic moment rates using the global NEIC
637 catalogue and local GNSS data for both the magma-poor Corinth Rift and magma-rich
638 Danakil Depression. Using determined moment rates we calculated the seismic/geodetic
639 moment rate ratios (S/G) for the entire rifts and for overlapping zones along each rift to
640 quantify the proportion of extension that is accommodated by seismic deformation. We
641 find:

642 • The seismic/geodetic moment rate ratio (S/G) is greater at the Corinth Rift (0.43)
643 compared with the Danakil Depression (0.03), indicating that greater amounts of
644 extension are being accommodated by faulting in the Corinth Rift. This is consistent with
645 the hypothesis that in magma-poor rifts, a greater proportion of deformation is seismic
646 (brittle faulting), while in magma-rich rifts aseismic magmatic intrusion is dominant.
647 • Extracting the horizontal component of the seismic moment rates, which improves
648 accuracy of comparison with the geodetic moment rates, produces values for the
649 horizontal seismic/geodetic moment rate ratio (S_h/G) of 0.02 for the Danakil Depression
650 and 0.28 for the Corinth Rift.
651 • Along rift variations in the S/G values in the Danakil Depression are consistent with
652 geological indicators of the varying contribution of faulting along the rift, e.g., axial
653 grabens and magmatic segments. In the north, a relatively high S/G of ~0.1 (~0.06
654 S_h/G), and likely an underestimation, indicates that brittle deformation accommodates a
655 significant amount of extension in this region despite being a magma-rich rift in the final

stages of break-up. In contrast, in the centre of the Danakil Depression, where the magmatic segments are located, the S/G is <0.05 (<0.03 S_h/G).

- There is significant discrepancy between the geodetic and seismic moment rates in the west of the Corinth Rift, with S/G ~0.1-0.15 (~0.07-0.1 S_h/G), and this likely cannot be fully accounted for by earthquake events missing from the seismicity catalogue. Therefore, this may be an indication of aseismic deformation occurring in the west of the Corinth Rift, potentially along a previously postulated immature low-angle detachment at depth.
- S/G values in the north of the Danakil Depression and the west of the Corinth Rift are similar (~0.1-0.15), therefore despite being magma-rich/magma-poor rift end members, regions within each of the rifts have similar amounts of seismic deformation (i.e., brittle faulting).

CRediT authorship contribution statement

Gareth L. Hurman: Writing – Original Draft, Methodology, Visualization, Investigation. **Derek Keir:** Conceptualization, Methodology, Supervision, Writing – Review & Editing. **Lisa C. McNeill:** Conceptualization, Supervision, Writing – Review & Editing. **Carolina Pagli:** Conceptualization, Writing – Review & Editing. **Jonathan M. Bull:** Conceptualization, Supervision, Writing – Review & Editing. **Georgios Michas:** Writing – Review & Editing.

Data availability

The National Earthquake Information Centre (NEIC) catalogue for the Danakil Depression and Corinth Rift was sourced from https://earthquake.usgs.gov/ and last accessed on 20/11/2023. The local seismicity catalogues for the Danakil Depression were sourced from the studies of Belachew et al. (2011) and Illsley-Kemp et al. (2018), with the catalogues available in an Open Access Publication (Zwaan et al, 2020a) available at https://doi.org/10.5880/fidgeo.2020.017. The local seismicity catalogue for the Corinth Rift was sourced from Hellenic Unified Seismic Network (HUSN) and available at https://bbnet.gein.noa.gr/HL/databases/database and was last accessed on 30/06/2023. GNSS data from the Afar region is attributed to Viltres et al. (2020). GNSS data for the Corinth Rift is from Avallone et al. (2004).

Acknowledgements

GH is supported by the Natural Environmental Research Council (NERC) through NERC Grant NE/S00721/1. CP and DK are partly supported by the Italian Ministero dell'Università e della Ricerca (MiUR) through PRIN Grant 2017P9AT72.

References

Ahmed, A., Doubre, C., Leroy, S., Keir, D., Pagli, C., Hammond, J. O. S., Ayele, A., de Berc, M, B, Grunberg, M., Vergne, J., Pestourie, R., Mamo, D., Kibret, B., Cubas, N., Lavayssière, A., Janowski, M., Lengliné, O., La Rosa, A., Chambers, E. L., Illsley-Kemp, F., 2022. Across and along-strike crustal structure variations of the Western Afar margin and adjacent plateau: Insights from receiver functions analysis. Journal of African Earth Sciences, 192, 104570. https://doi.org/10.1016/j.jafrearsci.2022.104570

Anderson, A. M., 1951. The dynamics of faulting and dike formation with application to Britain (2nd ed). Oliver and Boyd.

Armijo, R., Meyer, B., King, G. C. P., Rigo, A., Papanastassiou, D., 1996. Quaternary evolution of the Corinth Rift and its implications for the Late Cenozoic evolution of the Aegean. Geophysical Journal International, 126 (1), 11–53. https://doi.org/10.1111/j.1365-246X.1996.tb05264.x

Armijo, R., Meyer, B., Hubert, A. Barka, A., 1999. Westward propagation of the North Anatolian fault into the northern Aegean: Timing and kinematics. Geology, 27 (3) 267–270. https://doi.org/10.1130/0091-7613(1999)027<0267:WPOTNA>2.3.CO;2

Avallone, A., Briole, P., Agatza-Balodimou, A. M., Billiris, H., Charade, O., Mitsakaki, C, Nercessian, A., Papazissi, L., Paradissis, D., Veis, G., 2004. Analysis of eleven years of deformation measured by GPS in the Corinth Rift Laboratory area. Comptes Rendus Geoscience, 336, 301–311. https://doi.org/10.1016/j.crte.2003.12.007

Ayele, A., Stuart, G., Bastow, I., Keir, D., 2007. The August 2002 earthquake sequence in north Afar: Insights into the neotectonics of the Danakil microplate. Journal of African Earth Sciences, 48, 70–79. https://doi.org/10.1016/j.jafrearsci.2006.06.011

712 Barberi, F., Varet, J., 1970. The Erta-Ale volcanic range (Danakil Depression, northern Afar,
713 Ethiopia). Bulletin Volcanologique, 34 (4), 848–917. https://doi.org/10.1007/BF02596805

714 Bastow, I. D., Booth, A. D., Corti, G., Keir, D., Magee, C., Jackson, C. A.-L., Warren, J.,
715 Wilkinson, J., Lascialfari, M., 2018. The development of late-stage continental breakup:
716 Seismic reflection and borehole evidence from the Danakil Depression, Ethiopia. Tectonics,
717 37 (9), 2848–2862. https://doi.org/10.1029/2017TC004798

718 Belachew, M., Ebinger, C., Coté, D., Keir, D., Rowland, J. V., Hammond, J. O. S., Ayele, A.,
719 2011. Comparison of dike intrusions in an incipient seafloor-spreading segment in Afar,
720 Ethiopia: Seismicity perspectives. Journal of Geophysical Research, 116 (B6), B06405.
721 https://doi.org/10.1029/2010JB007908

722 Bell, R. E., McNeill, L. C., Henstock, T., Bull, J. M., 2011. Comparing extension on multiple
723 time and depth scales in the Corinth Rift, Central Greece. Geophysical Journal International,
724 186, 463–470. https://doi.org/10.1111/j.1365-246X.2011.05077.x

725 Bell, R. E., McNeill, L. C., Bull, J. M., Henstock, T., Collier, R. E. L., Leeder, M. R., 2009. Fault
726 architecture, basin structure and evolution of the Gulf of Corinth Rift, central Greece. Basin
727 Research, 21, 824–855. https://doi.org/10.1111/j.1365-2117.2009.00401.x

728 Bell, R. E., Duclaux, G., Nixon, C. W., Gawthorpe, R. L., McNeill, L. C., 2018. High angle, not
729 low-angle, normal faults dominate early rift extension in the Corinth Rift, central Greece.
730 Geology, 46, 115–118. https://doi.org/10.1130/G39560.1

731 Bernard, P., Briole, P., Meyer, B., Lyon-Caen, H., Gomez, J.-M., Tiberi, C., Berge, C., Cattin, R.,
732 Hatzfeld, D., Lachet, C., Lebrun, B., Deschamps, A., Courboulex, F., Larroque, C., Rigo, A.,
733 Massonnet, D., Papadimitriou, P., Kassaras, J., Diagourtas, D., Makropoulos, K., Veis, G.,
734 Papazisi, E., Mitsakaki, C., Karakostas, V., Papadimitriou, E., Papanastassiou, D., Chouliaras,
735 M., Stavrakakis, G., 1997. The Ms = 6.2, June 15 1995 Aigion earthquake (Greece): evidence
736 for low angle normal faulting in the Corinth Rift. Journal of Seismology, 1 (2), 131–150.
737 https://doi.org/10.1023/A:1009795618839

738 Bernard, P., Lyon-Caen, H., Briole, P., Deschamps, A., Boudin, F., Makropoulos, K.,
739 Papadimitriou, P., Lemeille, F., Patau, F., Billiris, H., Paradissis, D., Papazissi, K., Castarède,
740 H., Charade, O., Nercessian, A., Avallone, A., Pacchiani, F., Zahradnik, J., Sacks, S., Linde, A.,

741 2006. Seismicity, deformation and seismic hazard in the western rift of Corinth: new insights
742 from the Corinth Rift Laboratory (CRL). Tectonophysics, 426 (1–2), 7–30.
743 https://doi.org/10.1016/j.tecto.2006.02.012

744 Briole, P. Rigo, A., Lyon-Caen, H., Ruegg, J. C., Papazissi, K., Mitsakaki, C., Balodimou, A.,
745 Veis, G., Hatzeld, D., Deschamps, A., 2000. Active deformation of the Corinth rift, Greece:
746 Results from repeated Global Positioning System surveys between 1990 and 1996. Journal
747 of Geophysical Research, 105 (B11), 25605–25625. https://doi.org/10.1029/2000JB900148

748 Brinckmann, J., Kürsten, M., 1971. Stratigraphie und Tektonik der Danakil-Senk (NE-
749 Ätiopien). Beihefte Geol. Jahrb, 116, 5-87.

750 Buck, W., 2006. The role of magma in the development of the Afro-Arabian Rift System, in:
751 Yirgu, G., Ebinger, C. J., Maguire, P. K. H. (Eds.), The Afar volcanic province within the East
752 African Rift system. Geological Society of London, Special Publication 259, 43–54.
753 https://doi.org/10.1144/GSL.SP.2006.259.01.05

754 Buck, W., 2017. The role of magmatic loads and rift jumps in generating seaward dipping
755 reflectors on volcanic rifted margins. Earth and Planetary Science Letters, 466, 62–69.
756 https://doi.org/10.1016/j.epsl.2017.02.041

757 Chousianitis, K., Ganas, A., Evangelidis, C. P., 2015. Strain and rotation rate patterns of
758 mainland Greece from continuous GPS data and comparison between seismic and geodetic
759 moment release. Journal of Geophysical Research: Solid Earth, 120, 3909–3931.
760 https://doi.org/10.1002/2014JB011762

761 Corti, G., Agostini, A., Keir, D., Van Wijk, J., Bastow, I. D., Ranalli, G., 2015. Magma-induced
762 axial subsidence during final-stage rifting: Implications for the development of seaward-
763 dipping reflectors. Geosphere, 11 (3), 563–571. https://doi.org/10.1130/GES01076.1

764 Clarke, P. J., Davies, R. R., England, P. C., Parsons, B. E., Billiris, H., Paradissis, D., Veis, G.,
765 Denys, P. H., Cross, P. A., Ashkenazi, V., Bingley, R., 1997. Geodetic estimate of seismic
766 hazard in the Gulf of Korinthos. Geophysical Research Letters, 24, 1303–1306.
767 https://doi.org/10.1029/97GL01042

768 Clarke, P. J., Davies, R. R., England, P. C., Parsons, B., Billiris, H., Paradissis, D., Veis, G., Cross,
769 P. A., Denys, P. H., Ashkenazi, V., Bingley, R., Kahle, H. –G., Muller, M. –V., Briole, P., 1998.

770 Crustal strain in central Greece from repeated GPS measurements in the interval 1989–
771 1997. Geophysical Journal International, 135, 195–214. https://doi.org/10.1046/j.1365-
772 246X.1998.00633.x

773 De Barros, L., Cappa, F., Deschamps, A., Dublanchet, P., 2020. Imbricated aseismic slip and
774 fluid diffusion drive a seismic swarm in the Corinth Gulf, Greece. Geophysical Research
775 Letters, 47, e2020GL087142. https://doi.org/10.1029/2020GL087142

776 De Martini, P. M, Pantosti, D., Palyvos, N., Lemeille, F., McNeill, L. C., Collier, R., 2004. Slip
777 rates of the Aigion and Eliki Faults from uplifted marine terraces, Corinth Gulf, Greece.
778 Tectonics, 336, 325–334. https://doi.org/10.1016/j.crte.2003.12.006

779 Déprez, A., Doubre, C., Masson, F., Ulrich, P., 2013. Seismic and aseismic deformation along
780 the East African Rift System from a reanalysis of the GPS velocity field of Africa. Geophysical
781 Journal International, 193, 153–1369. https://doi.org/10.1093/gji/ggt085

782 Doutsos, T., Kontopoulos, N., Poulimenos, G., 1988. The Corinth-Patras rift as the initial
783 stage of continental fragmentation behind an active island arc (Greece). Basin Research, 1
784 (3), 177–190. https://doi.org/10.1111/j.1365-2117.1988.tb00014.x

785 Duverger, C., Godano, M., Bernard, P., Lyon-Caen, H., Lambotte, S., 2015. The 2003-2004
786 seismic swarm in the western Corinth rift: Evidence for a multiscale pore pressure diffusion
787 process along a permeable fault system. Geophysical Research Letters, 42, 7374–7382.
788 https://doi.org/10.1002/2015GL065298

789 Duverger, C., Lambotte, S., Bernard, P., Lyon-Caen, H., Deschamps, A., Nercessian, A., 2018.
790 Dynamics of micro-seismicity and its relationship with the active structures in the western
791 Corinth Rift (Greece). Geophysical Journal International, 215 (1), 196–221.
792 https://doi.org/10.1093/gji/ggy264

793 Eagles, G., Gloaguen, R., Ebinger, C., 2002. Kinematics of the Danakil microplate. Earth and
794 Planetary Science Letters, 203 (2), 607–620. https://doi.org/10.1016/S0012-821X(02)00916-
795 0

796 Ebinger, C. J., Oliva, S. J., Pham, T. –Q., Peterson, K., Chindandali, P., Illsley-Kemp, F., Drooff,
797 C., Shillington, D. J., Accardo, N. J., Gallacher, R. J., Gaherty, J., Nyblade, A. A., Mulibo, G.,
798 2019. Kinematics of Active Deformation in the Malawi Rift and Rungwe Volcanic Province,

Africa. Geochemistry, Geophysics, Geosystems, 20, 3928–3951. https://doi.org/10.1029/2019GC008354

Ehrhardt, A., Hübscher, C., 2015. The Northern Red Sea in transition from rifting to drifting-lessons learned from ocean deeps, in: Rasul, N. M. A., Stewart, I. C. F. (Eds.), The Red Sea: the formation, morphology, oceanography and environment of a young ocean basin. Springer Earth System Sciences, Heidelberg, pp. 99–121. https://doi.org/10.1007/978-3-662-45201-1_5

Franke, D., 2013. Rifting, lithosphere breakup and volcanism: Comparison of magma-poor and volcanic rifted margins. Marine and Petroleum Geology, 43, 63–87. https://doi.org/10.1016/j.marpetgeo.2012.11.003

Ford, M., Hemelsdaël, R., Mancini, M., Palyvos, N., 2017. Rift migration and lateral propagation: evolution of normal faults and sediment-routing systems of the western Corinth rift (Greece), in: Childs, C., Holdsworth, R. E., Jackson, C. A.-L., Manzocchi, T., Walsh, J. J., Yielding, G. (Eds.), The Geometry and Growth of Normal Faults. Geological Society of London, Special Publication 439, 131–168. https://doi.org/10.1144/SP439.15

Ford, M., Rohais, S., Williams, E., A., Bourlange, S., Jousselin, D., Backert, N., Malartre, F., 2013. Tectono-sedimentary evolution of the western Corinth Rift (Central Greece). Basin Research, 25 (1), 3–25. https://doi.org/10.1111/j.1365-2117.2012.00550.x

Gawthorpe, R., Leeder, M, R., Kranis, H., Skourtsos, E., Andrews, J. E., Henstra, G. A., Mack, G. H., Muravchik, M., Turner, J., A., Stamatakis, M., 2017. Tectono-sedimentary evolution of the Plio-Pleistocene Corinth rift, Greece. Basin Research, 30 (3), 448–479. https://doi.org/10.1111/bre.12260

Goitom, B., Oppenheimer, C., Hammond, J. O. S., Grandin, R., Barnie, T., Donovan, A., Ogubazghi, G., Yohannes, E., Kibrom, G., Kendall, J-. M., Carn, S. A., Free, D., Sealing, C., Keir, D., Ayele, A., Blundy, J., Hamlyn, J., Wright, T., Berhe, S., 2015. First recorded eruption of Nabro volcano, Eritrea, 2011. Bulletin of Volcanology, 77 (10), 1–21. https://doi.org/10.1007/s00445-015-0966-3

Hammond, J. O. S., Kendall, J.-M., Stuart, G. W., Keir, D., Ebinger, C., Ayele, A., Belachew, M., 2011. The nature of the crust beneath the Afar triple junction: Evidence from receiver

functions. Geochemistry, Geophysics, Geosystems, 12 (12). https://doi.org/10.1029/2011GC003738

Hamlyn, J. E., Keir, D., Wright, T. J., Neuberg, J. W., Goitom, B., Hammond, J. O. S., Pagli, C., Oppenheimer, C., Kendall, J-. M., Grandin, R., 2014. Seismicity and subsidence following the 2011 Nabro eruption, Eritrea: Insights into the plumbing system of an off-rift volcano. Journal of Geophysical Research: Solid Earth, 119, 8267–8282. https://doi.org/10.1002/2014JB011395

Hatzfeld, D., Kementzetzidou, D., Karakostas, V., Ziazia, M., Nothard, S., Diagourtas, D., Deschamps, A., Karakaisis, G., Papadimitriou, P., Scordilis, M., Smith, R., Voulgaris, N., Kiratzi, S., Makropoulos, K., Bouin, M. P., Bernard, P., 1996. The Galaxidi earthquake of 18 November 1992: a possible asperity within the normal fault system of the Gulf of Corinth (Greece). Bulletin of the Seismological Society of America, 86 (6), 1987–1991. https://doi.org/10.1785/BSSA0860061987

Hayward, N. J., Ebinger, C. J., 1996. Variations in the along-axis segmentation of the Afar Rift system. Tectonics, 15 (2), 244–257. https://doi.org/10.1029/95TC02292

Hofmann, C., Courtillot, V., Féraud, G., Rochette, P., Yirgu, G., Ketefo, E., Pik, R., 1997. Timing of the Ethiopian flood basalt event and implications for plume birth and global change. Nature, 389 (6653), 838–841. https://doi.org/10.1038/39853

Hurman, G. L., Keir, D., Bull, J. M., McNeill, L. C., Booth, A. D., Bastow, I. D., 2023 Quantitative analysis of faulting in the Danakil Depression Rift of Afar: The importance of faulting in the final stages of magma-rich rifting. Tectonics, 42 (6), e2022TC007607. https://doi.org/10.1029/2022TC007607

Illsley-Kemp, F., Keir, D., Bull, J., Gernon, T., Ebinger, C., Ayele, A., Hammond, J. O. S., Kendall, J-. M., Goitom, B., Belachew, M., 2018. Seismicity during continental breakup in the Red Sea rift of Northern Afar. Journal of Geophysical Research: Solid Earth, 123 (3), 2345–2362. https://doi.org/10.1002/2017JB014902

Jackson, J.A., Gagnepain, J., Houseman, G., King, G.C.P., Papadimitriou, P., Soufleris, C., Virieux, J., 1982. Seismicity, normal faulting, and the geomorphological development of the

856 Gulf of Corinth (Greece): the Corinth earthquakes of February & March 1981. Earth and
857 Planetary Science Letters, 57, 377-397. https://doi.org/10.1016/0012-821X(82)90158-3

858 Jenny, S., Goes, S., Giardini, D., Kahle, H. –G., 2004. Earthquake recurrence parameters from
859 seismic and geodetic strain rates in eastern Mediterranean. Geophysical Journal
860 International, 157, 1331–1347. https://doi.org/10.1111/j.1365-246X.2004.02261.x

861 Jolivet, L., Daniel, J. M., Truffert, C., Goffe, B., 1994. Exhumation of deep crustal
862 metamorphic rocks and crustal extension in arc and back-arc regions. Lithos, 33 (1-3), 3–30.
863 https://doi.org/10.1016/0024-4937(94)90051-5

864 Kanamori, H., 1977. The energy release in great earthquakes. Journal of Geophysical
865 Research, 82, 1981–1987. https://doi.org/10.1029/JB082i020p02981

866 Kapetanidis, V., Deschamps, A., Papadimitriou, P., Matrullo, E., Karakonstantis, A.,
867 Bozionelos, G., Kaviris, G., Serpetsidaki, A., Lyon-Caen, H., Voulgaris, N., Bernard, P., Sokos,
868 E., Makropoulos, K., 2015. The 2013 earthquake swarm in Helike, Greece: seismic activity at
869 the root of old normal faults. Geophysical Journal International, 202 (3), 2044–2073.
870 https://doi.org/10.1093/gji/ggv249

871 Kapetanidis, V., Michas, G., Kaviris, G. Vallianatos, F., 2021. Spatiotemporal Properties of
872 Seismicity and Variations of Shear-Wave Splitting Parameters in the Western Gulf of Corinth
873 (Greece). Applied Sciences, 11 (14), 6573. https://doi.org/10.3390/app11146573

874 Kaviris, G., Elias, P., Kapetanidis, V., Serpetsidaki, A., Karakonstantis. A., Vladimír Plicka, V.,
875 De Barros, L., Sokos, E., Kassaras, I., Sakkas, V., Spingos, I., Lambotte, S., Duverger, C.,
876 Lengliné, O., Evangelidis, C. P., Fountoulakis, I., Ktenidou, O. –J., Gallovič, F., Bufféral, S.,
877 Klein, E., Aissaoui, E. M., Scotti, O., Lyon-Caen, H., Rigo, A., Papadimitriou, P., Voulgaris, N.,
878 Zahradnik, J., Deschamps, A., Briole, P., Bernard, P., 2021. The Western Gulf of Corinth
879 (Greece) 2020–2021 Seismic Crisis and Cascading Events: First Results from the Corinth Rift
880 Laboratory Network. The Seismic Record, 1 (2), 85–95. https://doi.org/10.1785/0320210021

881 Kaviris, G., Spingos, I., Kapetanidis, V., Papadimitriou, P., Voulgaris, N., Makropoulos, K.,
882 2017. Upper crust seismic anisotropy study and temporal variations of shear-wave splitting
883 parameters in the western Gulf of Corinth (Greece) during 2013. Physics of the Earth and
884 Planetary Interiors, 269, 148–164. https://doi.org/10.1016/j.pepi.2017.06.006

885 Keir, D., Bastow, I. D., Corti, G., Mazzarini, F., Rooney, T. O., 2015. The origin of along-rift
886 variations in faulting and magmatism in the Ethiopian Rift. Tectonics, 34 (3), 464–477.
887 https://doi.org/10.1002/2014TC003698

888 Keir, D., Bastow, I. D., Pagli, C., Chambers, E. L., 2013. The development of extension and
889 magmatism in the Red Sea rift of Afar. Tectonophysics, 607, 98–114.
890 https://doi.org/10.1016/j.tecto.2012.10.015

891 Koukouvelas, I. K., Stamatopoulos, L., Katsonopoulou, D., Pavlides, S., 2001. A
892 palaeoseismological and geoarchaeological investigation of the Eliki fault, Gulf of Corinth,
893 Greece. Journal of Structural Geology, 23, 531–543. https://doi.org/10.1016/S0191-
894 8141(00)00124-3

895 Kostrov. B., 1974. Seismic moment and energy of earthquakes and seismic flow of rock,
896 Izvestiya, Academy of Sciences, USSR Phys. Solid Earth, 1, 23–40.

897 La Rosa, A., Raggiunti, M., Pagli, C., Keir, D, Wang, H., Ayele, A., 2023. Extensional
898 Earthquakes in the Absence of Magma in Northern Afar: Insights From InSAR. Geophysical
899 Research Letters, 50, e2023GL102826. https://doi.org/10.1029/2023GL102826

900 La Rosa, A., Pagli, C., Wang, H., Doubre, C., Leroy, S., Sani, F., Corti, G., Ayele, A., Keir, D.
901 2021a. Plate-boundary kinematics of the Afrera linkage zone (Afar) from InSAR and
902 seismicity. Journal of Geophysical Research: Solid Earth, 126,
903 e2020JB021387. https://doi.org/10.1029/2020JB021387

904 La Rosa, A., Keir, D., Doubre, C., Sani, F., Corti, G., Leroy, S., Ayele, A., Pagli, C. 2021b. Lower
905 crustal earthquakes in the March 2018 sequence along the Western Margin of Afar.
906 Geochemistry, Geophysics, Geosystems, 22, e2020GC009614.
907 https://doi.org/10.1029/2020GC009614

908 Lambotte, S., Lyon-Caen, H., Bernard, P., Deschamps, A., Patau, G., Nercessian, A., Pacchiani,
909 F., Bourouis, S., Drilleau, M., Adamova, P., 2014. Reassessment of the rifting process in the
910 Western Corinth Rift from relocated seismicity. Geophysical Journal International, 197 (3),
911 1822–1844. https://doi.org/10.1093/gji/ggu096

912 Lavayssière, A., Drooff, C., Ebinger, C., Gallacher, R., Illsley-Kemp, F., Olivia, S. J., Keir, D.,
913 2019. Depth Extent and Kinematics of Faulting in the Southern Tanganyika Rift, Africa.
914 Tectonics, 38, 842–862. https://doi.org/10.1029/2018TC005379

915 Lavier, L. L., Manatschal, G., 2006. A mechanism to thin the continental lithosphere at
916 magma-poor margins. Nature, 440 (7082), 324–328. https://doi.org/10.1038/nature04608

917 Le Gall, B., Leleu, S., Pik, R., Jourdan, F., Chazot, G., Ayalew, D., Yirgu, G., Cloquet, C., and
918 Chauvet, F., 2018. The Red Beds Series in the Erta Ale segment, North Afar. Evidence for a 6
919 Ma-old post-rift basin prior to continental rupturing. Tectonophysics, 747–748, 373– 389.
920 https://doi.org/10.1016/j.tecto.2018.10.00

921 Le Pourhiet, L., Burov, E., Moretti, I., 2003. Initial crustal thickness geometry controls on the
922 extension in a back arc domain: Case of the Gulf of Corinth. Tectonics, 22 (4), 1032.
923 https://doi.org/10.1029/2002TC001433

924 Makris, J., Ginzburg, A., 1987. The Afar depression: Transition between continental rifting
925 and sea-floor spreading. Tectonophysics, 141 (1-3), 199–214. https://doi.org/10.1016/0040-
926 1951(87)90186-7

927 Manighetti, I., Tapponnier, P., Courtillot, V., Gallet, Y., Jacques, E., Gillot, P. –Y., 2001. Strain
928 transfer between disconnected, propagating rifts in Afar. Journal of Geophysical Research:
929 Solid Earth, 106 (B7), 13613–13665. https://doi.org/10.1029/2000JB900454

930 McClusky, S., Balassanian, S., Barka, A., Demir, C., Ergintav, S., Georgiev, I., Gurkan, O.,
931 Hamburger, M., Hurst, K., Kahle, H., Kastens, K., Kekelidze, G., King, R., Kotzev, V., Lenk, O.,
932 Mahmoud, S., Mishin, A., Nadariya, M., Ouzounis A., Paradissis, D., Peter, Y., Prilepin, M.,
933 Reilinger, R., Sanli, I., Seeger, H., Tealeb, A., Toksöz, M.N., Veis, G., 2000. Global Positioning
934 System constraints on plate kinematics and dynamics in the eastern Mediterranean and
935 Caucasus. Journal of Geophysical Research: Solid Earth, 105 (B3), 5695–5719.
936 https://doi.org/10.1029/1999JB900351

937 McClusky, S., Reilinger, R., Ogubazghi, G., Amleson, A., Healeb, B., Vernant, P., Sholan, J.,
938 Fisseha, S., Asfaw, L., Bendick, R., Kogan, L., 2010. Kinematics of the southern Red Sea–Afar
939 Triple Junction and implications for plate dynamics. Geophysical Research Letters, 37 (5).
940 https://doi.org/10.1029/2009GL041127

McKenzie, D., Davies, D., Molnar, P., 1970. Plate tectonics of the Red Sea and East Africa. Nature, 226 (5242), 243–248. https://doi.org/10.1038/226243a0

McNeill, L. C., Collier R. E. L., 2004. Uplift and slip rates of the eastern Eliki fault segment, Gulf of Corinth, Greece, inferred from Holocene and Pleistocene terraces. Journal of the Geological Society, 161 (1), 81–92. https://doi.org/10.1144/0016-764903-029

McNeill, L. C., Collier, R. E. Ll., De Martini, P. M., Pantosti, D. & D'Addezio, G., 2005. Recent history of the Eastern Eliki Fault, Gulf of Corinth: geomorphology, palaeoseismology and impact on palaeoenvironments. Geophysical Journal International, 161, 154–166. https://doi.org/10.1111/j.1365-246X.2005.02559.x

McNeill, L. C., Shillington, D. J., Carter, G. D. O., and the Expedition 381 Participants, 2019a. Corinth Active Rift Development. Proceedings of the International Ocean Discovery Program, 381: College Station, TX (International Ocean Discovery Program). https://doi.org/10.14379/iodp.proc.381.2019

McNeill, L. C., Shillington, D. J., Carter, G. D. O., Everest, J. D., Gawthorpe, R. L., Miller, C., Phillips, M. P., Collier, R. E. Ll., Cvetkoska, A., De Gelder, G., Diz, P., Doan, M.-L., Ford, M., Geraga, M., Gillespie, J., Hemelsdaël, R., Herrero-Bervera, E., Ismaiel, M., Janikian, L., Kouli, K., Le Ber, E., Li, S., Maffione, M., Mahoney, C., Machlus, M. L., Michas, G., Nixon, C. W., Oflaz, S. A., Omale, A. P., Panagiotopulos, K., Pechlivanidou, S., Sauer, S., Seguin, J., Sergious, S., Zakharova, N. V., Green, S., 2019b. High-resolution record reveals climate-driven environmental and sedimentary changes in an active rift. Scientific Reports, 9, 3116. https://doi.org/10.1038/s41598-019-40022-w

Mesimeri, M., Karakostas, V., Papadimitriou, E., Schaff, D., Tsaklidis, G., 2016. Spatio-temporal properties and evolution of the 2013 Aigion earthquake swarm (Corinth Gulf, Greece). Journal of Seismology, 20, 595–614. https://doi.org/10.1007/s10950-015-9546-4

Michas, G., Kapetanidis, V., Spingos, I., Kaviris, G., Vallianatos, F., 2022. The 2020 Perachora peninsula earthquake sequence (East Corinth Rift, Greece): spatiotemporal evolution and implications for the triggering mechanism. Acta Geophysica, 70, 2581–2601. https://doi.org/10.1007/s11600-022-00864-x

969 Moore, C., Wright, T., Hooper, A., Biggs, J., 2019. The 2017 eruption of Erta'Ale volcano,
970 Ethiopia: Insights into the shallow axial plumbing system of an incipient mid-ocean ridge.
971 Geochemistry, Geophysics, Geosystems, 20 (12), 5727–5743.
972 https://doi.org/10.1029/2019GC008692

973 Musila, M., Ebinger, C. J., Bastow, I. D., Sullivan, G., Oliva, S. J., Knappe, E., Perry, M.,
974 Kounoudis, R., Ogden, C. S., Bendick, R., Mwangi, S., Mariita, N., Kianji, G., Kraus, E., Illsley-
975 Kemp, F., 2023. Active Deformation Constraints on the Nubia-Somalia Plate Boundary
976 Through Heterogenous Lithosphere of the Turkana Depression. Geochemistry, Geophysics,
977 Geosystems, 24, e2023GC010982. https://doi.org/10.1029/2023GC010982

978 Nixon, C. W., McNeill, L. C., Bull, J. M., Bell, R. E., Gawthorpe, R. L., Henstock, T. J.,
979 Christodoulou, D., Ford, M., Taylor, B., Sakellariou, D., Ferentinos, G., Papatheodorou, G.,
980 Leeder, M. R., Collier, R. E. Ll., Goodliffe, A. M., Sachpazi, M., Kranis, H., 2016. Rapid
981 spatiotemporal variations in rift structure during development of the Corinth Rift, central
982 Greece. Tectonics, 35 (5), 1225–1248. https://doi.org/10.1002/2015TC004026

983 Nixon, C. W., McNeill, L. C, Gawthorpe, R. L., Shillington, D. J., Michas, G., Bell, R. E., Moyles,
984 A., Ford, M., Zakharova, N. V., Bull, J. M., de Gelder, G., 2024. Increasing fault slip rates
985 within the Corinth Rift, Greece: A rapidly localising active rift fault network. Earth and
986 Planetary Science Letter, 636, 118716. https://doi.org/10.1016/j.epsl.2024.118716

987 Nobile, A., Pagli, C., Keir, D., Wright, T. J., Ayele, A., Ruch, J., Acocella, V., 2012. Dike-fault
988 interaction during the 2004 Dallol intrusion at the northern edge of the Erta Ale Ridge (Afar,
989 Ethiopia). Geophysical Research Letters, 39 (19). https://doi.org/10.1029/2012GL053152

990 Pagli, C., Wang, H., Wright, T. J., Calais, E., Lewi, E., 2014. Current plate boundary
991 deformation of the Afar rift from a 3-D velocity field inversion of InSAR and GPS. Journal of
992 Geophysical Research: Solid Earth, 119 (11), 8562–8575.
993 https://doi.org/10.1002/2014JB011391

994 Pagli, C., Wright, T. J., Ebinger, C. J., Yun, S.-H., Cann, J. R., Barnie, T., Atalay, A., 2012.
995 Shallow axial magma chamber at the slow spreading Erta Ale Ridge. Nature Geoscience, 5
996 (4), 284–288. https://doi.org/10.1038/ngeo1414

997 Palano, M., Cannavò, F., Ferranti, L., Mattia, M., Mazzella, M. E., 2011. Strain and stress
998 fields in the Southern Apennines (Italy) constrained by geodetic, seismological and borehole
999 data. Geophysical Journal International, 197 (3), 1270-1282. https://doi.org/10.1111/j.1365-
1000 246X.2011.05234.x

1001 Pancha, A., Anderson, J. G., Kreemer. C., 2006. Comparison of seismic and geodetic scalar
1002 moment rates across the Basin and Range Province. Bulletin of the Seismological Society of
1003 America, 96, 11–32. https://doi.org/10.1785/0120040166

1004 Pantosti, D., De Martini, P. M., Koukouvelas, I., Stamatopulos, L., Palyvos, N, Pucci, S.,
1005 Lemaille, F., Pavlides, S., 2004. Palaeoseismological investigations of the Aigion Fault (Gulf of
1006 Corinth, Greece). Comptes Rendus Geoscience, 336 (4-5), 335-342.
1007 https://doi.org/10.1016/j.crte.2003.12.005

1008 Papadimitriou, E., Bonatis, P., Bountzis, P., Kostoglou, A., Kourouklas, C_H., Karakostas, V.,
1009 2022. The Intense 2020–2021 Earthquake Swarm in Corinth Gulf: Cluster Analysis and
1010 Seismotectonic Implications from High Resolution Microseismicity. Pure and Applied
1011 Geophysics, 179, 3121–3155. https://doi.org/10.1007/s00024-022-03135-4

1012 Pe-Piper, G., Piper, D. J. W., 2005. The South Aegean active volcanic arc: relationships
1013 between magmatism and tectonics. Developments in Volcanology, 7, 113-133.
1014 https://doi.org/10.1016/S1871-644X(05)80034-8

1015 Pérez-Gussinyé, M., Collier, J. S., Armitage, J. J., Hopper, J. R., Sun, Z., Ranero, C. R., 2023.
1016 Towards a process-based understanding of rifted continental margins. Nature Reviews Earth
1017 & Environment, 4, 166–184. https://doi.org/10.1038/s43017-022-00380-y

1018 Peron-Pinvidic, G., Manatschal, G., 2009. The final rifting evolution at deep magma-poor
1019 passive margins from Iberia-Newfoundland: A new point of view. International Journal of
1020 Earth Sciences, 98 (7), 1581–1597. https://doi.org/10.1007/s00531-008-0337-9

1021 Peron-Pinvidic, G., Manatschal, G., Osmundsen, P. T., 2013. Structural comparison of
1022 archetypal Atlantic rifted margins: A review of observations and concepts. Marine and
1023 Petroleum Geology, 43, 21–47. https://doi.org/10.1016/j.marpetgeo.2013.02.002

Pirazzoli, P. A., Stiros, S. C., Fontugne, M., Arnold, M., 2004. Holocene and Quaternary uplift in the central part of the southern coast of the Corinth Gulf (Greece). Marine Geology, 212 (1–4), 35–44. https://doi.org/10.1016/j.margeo.2004.09.006

Reston, T. J., 2009. The extension discrepancy and syn-rift subsidence deficit at rifted margins. Petroleum Geoscience, 15 (3), 217–237. https://doi.org/10.1144/1354-079309-845

Rime, V., Foubert, A., Ruch, J., Kidane, T., 2023. Tectonostratigraphic evolution and significance of the Afar Depression. Earth-Science Reviews, 244, 104519. https://doi.org/10.1016/j.earscirev.2023.104519

Sachpazi, M., Galvé, A., Laigle, M., Hirn, A., Sokos, E., Serpetsidaki, A., Marthelot, J. –M., Pi Aperin, J. M., Zelt, B., Taylor B., 2007. Moho topography under central Greece and its compensation by Pn time-terms for the accurate location of hypocenters: The example of the Gulf of Corinth 1995 Aigion earthquake. Tectonophysics, 440, 53–65. https://doi.org/10.1016/j.tecto.2007.01.009

Sakellariou, D., Lykousis, V., Alexandri, S., Kaberi, H., Rousakis, G., Nomikou, P., Georgiou, P. and Ballas, D., 2007. Faulting, seismic-stratigraphic architecture and Late Quaternary evolution of the Gulf of Alkyonides Basin-East Gulf of Corinth, Central Greece. Basin Research, 19 (2), 273-295. https://doi.org/10.1111/j.1365-2117.2007.00322.x

Sapin, F., Rigenback, J., -C., Clerc, C., 2021. Rifted margins classification and forcing parameters. Scientific Reports, 11, 8199. https://doi.org/10.1038/s41598-021-87648-3

Sawires, R., Peláez, J. A., Sparacino, F., Radwan, A. M., Rashwan, M. Palano. M., 2021. Seismic and Geodetic Crustal Moment-Rates Comparison: New Insights on the Seismic Hazard of Egypt. Applied Sciences, 11 (17), 7836. https://doi.org/10.3390/app11177836

Scordilis, E. M., 2006. Empirical global relations converting MS and mb to moment magnitude. Journal of Seismology, 10, 225–236. https://doi.org/10.1007/s10950-006-9012-4

Shillington, D. J., Scott, C. L., Minshull, T. A., Edwards, R. A., Brown, P. J., White, N., 2009. Abrupt transition from magma-starved to magma-rich rifting in the eastern Black Sea. Geology, 37 (1), 7–10. https://doi.org/10.1130/G25302A.1

Sparacino, F., Galuzzi, B. G., Palano, M., Segou, M., Chiarabba, C., 2022. Seismic coupling of the Aegean – Anatolian region. Earth-Science Reviews, 228, 103993. https://doi.org/10.1016/j.earscirev.2022.103993

Stewart, I., 1996. Holocene uplift and palaeoseismicity on the Eliki fault, Western Gulf of Corinth, Greece. Annals of Geophysics, 39 (3). https://doi.org/10.4401/ag-3993

Stewart, I., Vita-Finzi, C., 1996. Coastal uplift on active normal faults: the Eliki Fault, Greece. Geophysical Research Letters, 23 (14), 1853–1856. https://doi.org/10.1029/96GL01595

Szymanski, E., Stockli, D. F., Johnson, P. R., Hager, C., 2016. Thermochronometric evidence for diffuse extension and two-phase rifting within the Central Arabian Margin of the Red Sea Rift. Tectonics, 35 (12), 2863–2895. https://doi.org/10.1002/2016TC004336

Tesfaye, S., Harding, D., Kusky, T., 2003. Early continental breakup boundary and migration of the Afar triple junction, Ethiopia. Geological Society of America Bulletin, 115 (9), 1053–1067. https://doi.org/10.1130/B25149.1

Tiberi, C., Diament, M., Lyon-Caen, H., King, T., 2001. Moho topography beneath the Corinth Rift Area (Greece) from inversion gravity data. Geophysical Journal International, 145, 797–808. https://doi.org/10.1046/j.1365-246x.2001.01441.x

Tugend, J., Gillard, M., Manatschal, G., Nirrengarten, M., Harkin, C., Epin, M.-E., Sauter, D., Autin, J., Kusznir, N., McDermott, K., 2018. Reappraisal of the magma-rich versus magma-poor rifted margin archetypes, in: McClay, K. R., Hammerstein, J. A. (Eds.), Passive margins: Tectonic, sedimentation and magmatism. Geological Society of London, Special Publication 476, 23–47. https://doi.org/10.1144/SP476.9

Viltres, R., Jónsson, S., Ruch, J., Doubre, C., Reilinger, R., Floyd, M., Ogubazghi, G., 2020. Kinematics and deformation of the southern Red Sea region from GPS observations. Geophysical Journal International, 221 (3), 2143–2154. https://doi.org/10.1093/gji/ggaa109

Ward, S. N., 1998. On the consistency of earthquake moment release and space geodetic strain rates: Europe. Geophysical Journal International, 135, 1011–1018. https://doi.org/10.1046/j.1365-246X.1998.t01-2-00658.x

Watts, E. J., Gernon, T. M., Taylor, R. N., Keir, D., Pagli, C., 2023. Magmatic evolution during proto-oceanic rifting at Alu, Dalafilla and Borale Volcanoes (Afar) determined by trace element and Sr-Nd-Pb isotope geochemistry. Lithos, 456–457, 107311. https://doi.org/10.1016/j.lithos.2023.107311

Watts, E. J., Gernon, T. M., Taylor, R. N., Keir, D., Siegburg, M., Jarman, J., Pagli, C., Gioncada, A., 2020. Evolution of the Alu-Dalafilla and Borale volcanoes, Afar, Ethiopia. Journal of Volcanology and Geothermal Research, 408, 107094. https://doi.org/10.1016/j.jvolgeores.2020.107094

Weinstein, A., Oliva, S. J., Ebinger, C. J., Roecker, S., Tiberi, C., Aman, M., Lambert, C., Witkin, E., Albaric, J., Gautier, S., Peyrat, S., Muirhead, J. D., Muzuka, A. N. N., Mulibo, G., Kianji, G., Ferdinand-Wambura, R., Msabi, M., Rodzianko, A., Hadfield, R., Illsley-Kemp, F., Fischer, T. P., 2017. Fault-magma interactions during early continental rifting: Seismicity of the Magadi-Natron-Manyara basin, Africa. Geochemistry, Geophysics, Geosystems, 18, 3662–3686, https://doi.org/10.1002/2017GC007027

Wolfenden, E., Ebinger, C., Yirgu, G., Renne, P. R., Kelley, S. P., 2005. Evolution of a volcanic rifted margin: Southern Red Sea, Ethiopia. Geological Society of Amercia Bulletin, 117 (7–8), 846–864. https://doi.org/10.1130/B25516.1

Yirgu, G., Ebinger, C. J. Maguire, P. K. H., 2006. The Afar volcanic province within the East African Rift System: introduction, in: Yirgu, G., C. J. Ebinger, C J., Maguire, P. K. H. (Eds.), The Afar volcanic province within the East African Rift system (Vol. 259, pp. 106). Geological Society of London, Special Publication 259, 1–6. https://doi.org/10.1144/GSL.SP.2006.259.01.01

[dataset] Zwaan, F., Corti, G., Keir, D., Sani, F., Muluneh, A., Illsley-Kemp, F., Papini, M., 2020a. Geological data from the Western Afar margin, East Africa. GFZ Data Services. https://doi.org/10.5880/fidgeo.2020.017

Zwaan, F., Corti, G., Sani, F., Keir, D., Muluneh, A. A., Illsley-Kemp, F., Papini, M., 2020b. Structural analysis of the Western Afar margin, East Africa: Evidence for multiphase rotational rifting. Tectonics, 39 (7), e2019TC006043. https://doi.org/10.1029/2019TC006043

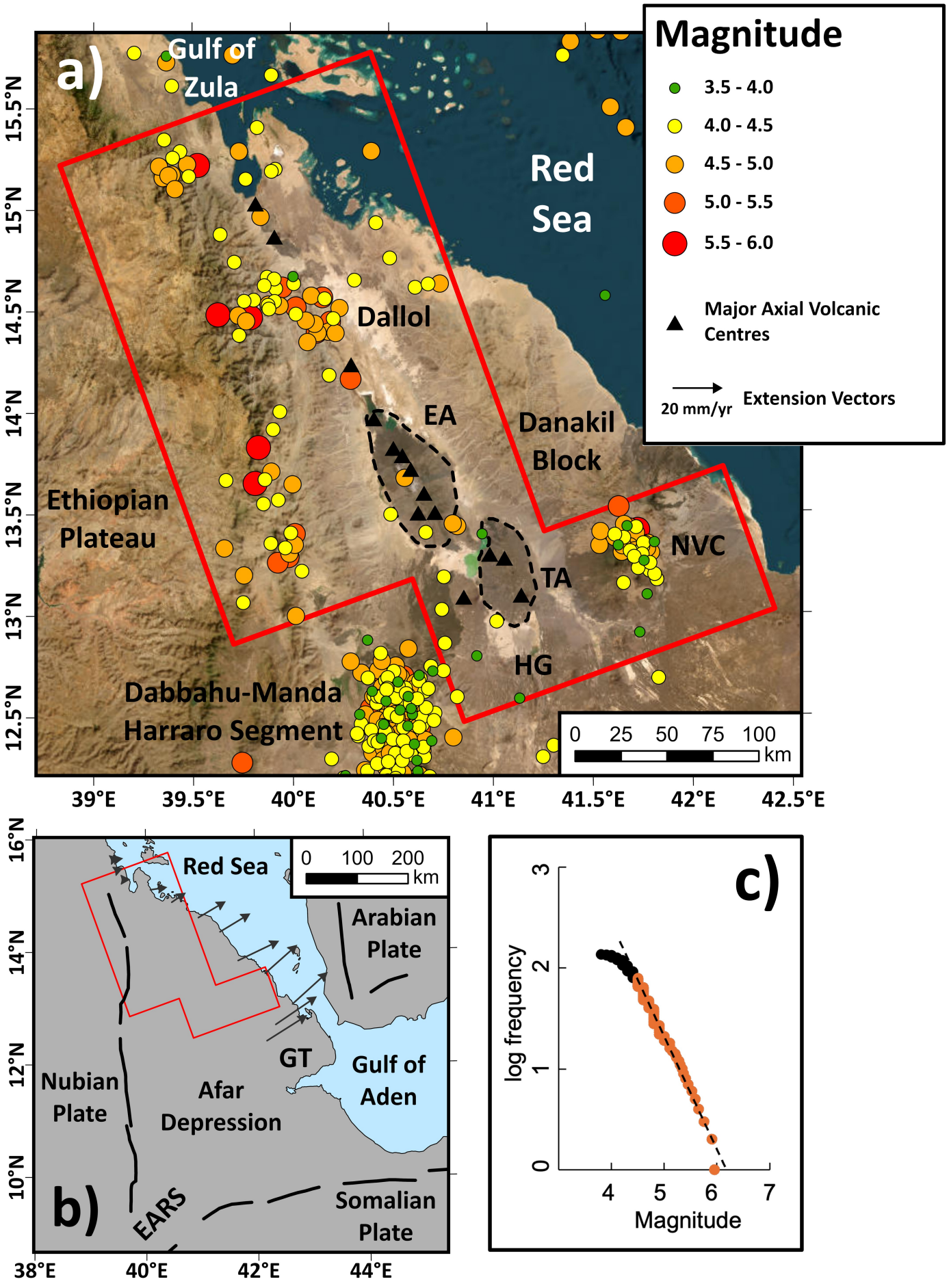
a)
Gulf of Zula
Red Sea
Dallol
EA
Danakil Block
Ethiopian Plateau
NVC
TA
HG
Dabbahu-Manda Harraro Segment
Magnitude
3.5 - 4.0
4.0 - 4.5
4.5 - 5.0
5.0 - 5.5
5.5 - 6.0
Major Axial Volcanic Centres
20 mm/yr
Extension Vectors
0 25 50 75 100 km
15.5°N
15°N
14.5°N
14°N
13.5°N
13°N
12.5°N
39°E
39.5°E
40°E
40.5°E
41°E
41.5°E
42°E
42.5°E
b)
Red Sea
0 100 200 km
Arabian Plate
GT
Gulf of Aden
Nubian Plate
Afar Depression
EARS
Somalian Plate
16°N
14°N
12°N
10°N
38°E
40°E
42°E
44°E
c)
log frequency
Magnitude
0
1
2
3
4
5
6
7

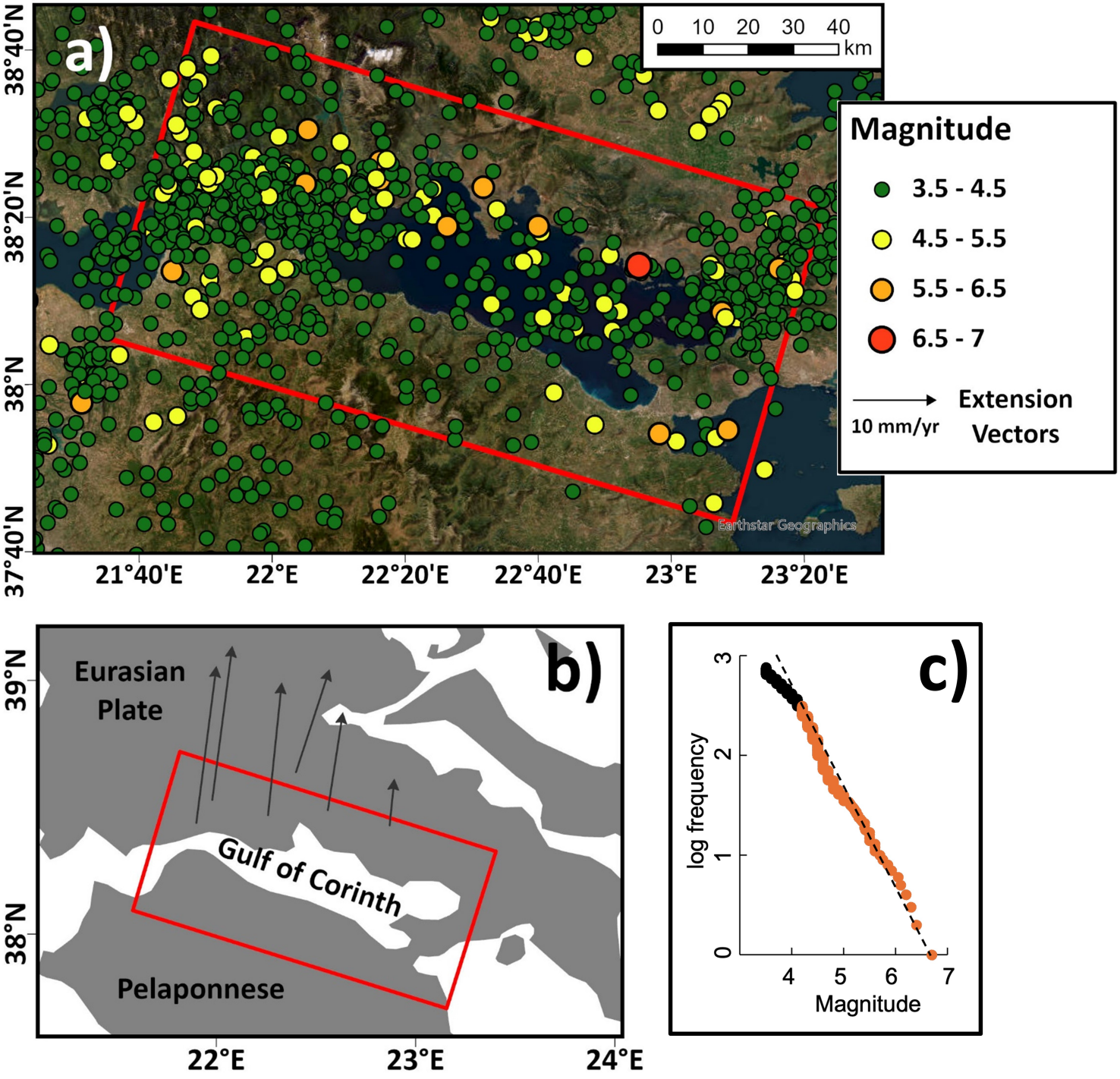
a)
0 10 20 30 40
km
Magnitude
3.5 - 4.5
4.5 - 5.5
5.5 - 6.5
6.5 - 7
Extension Vectors
10 mm/yr
Earthstar Geographics
38°40'N
38°20'N
38°N
37°40'N
21°40'E
22°E
22°20'E
22°40'E
23°E
23°20'E
b)
Eurasian Plate
Gulf of Corinth
Pelaponnese
39°N
38°N
22°E
23°E
24°E
c)
log frequency
Magnitude
0
1
2
3
4
5
6
7

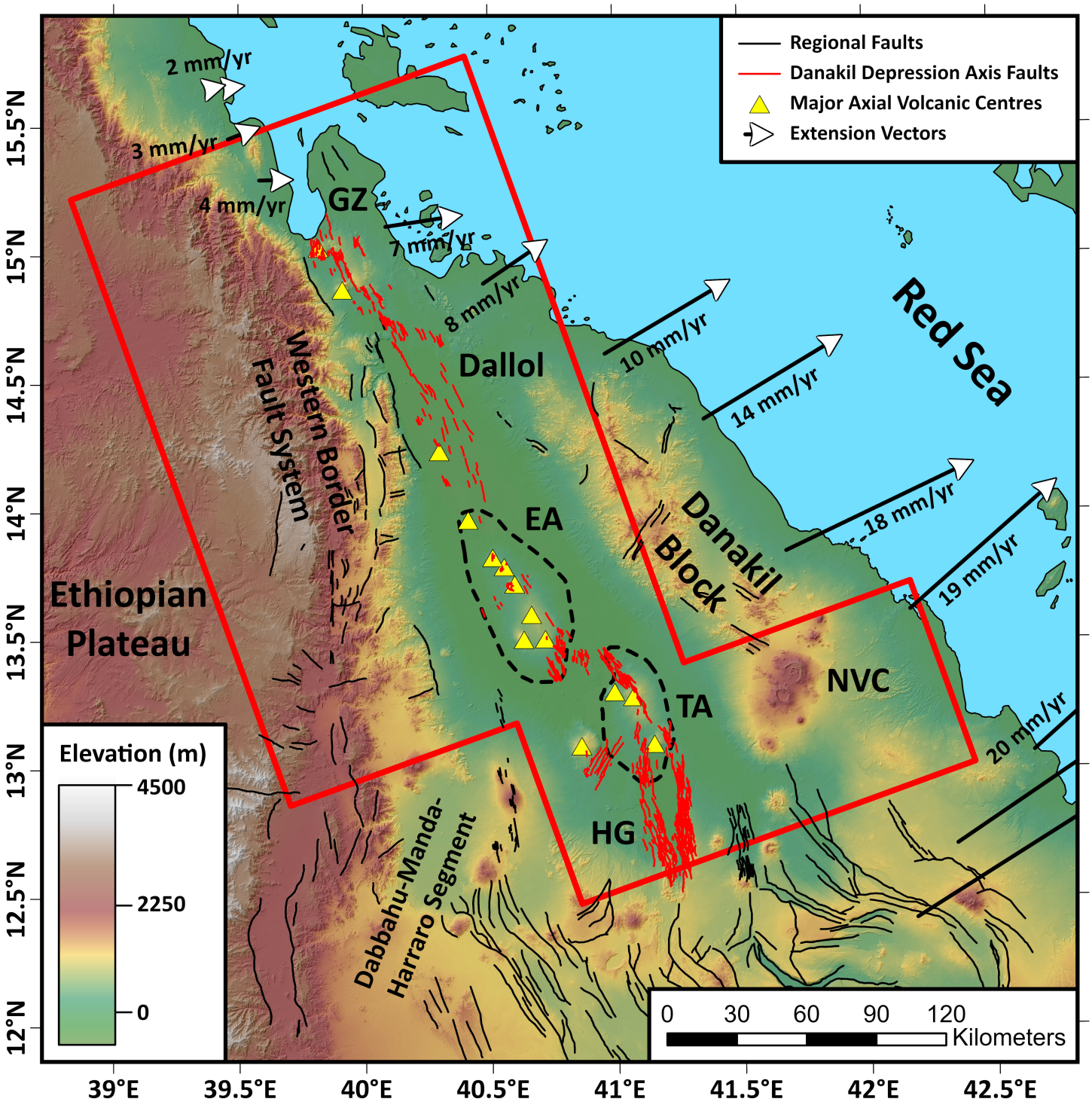
Regional Faults
Danakil Depression Axis Faults
Major Axial Volcanic Centres
Extension Vectors
2 mm/yr
3 mm/yr
4 mm/yr
7 mm/yr
8 mm/yr
10 mm/yr
14 mm/yr
18 mm/yr
19 mm/yr
20 mm/yr
GZ
Dallol
EA
TA
HG
NVC
Danakil Block
Red Sea
Western Border Fault System
Dabbahu-Manda-Harraro Segment
Ethiopian Plateau
Elevation (m)
4500
2250
0
0 30 60 90 120
Kilometers
15.5°N
15°N
14.5°N
14°N
13.5°N
13°N
12.5°N
12°N
39°E
39.5°E
40°E
40.5°E
41°E
41.5°E
42°E
42.5°E

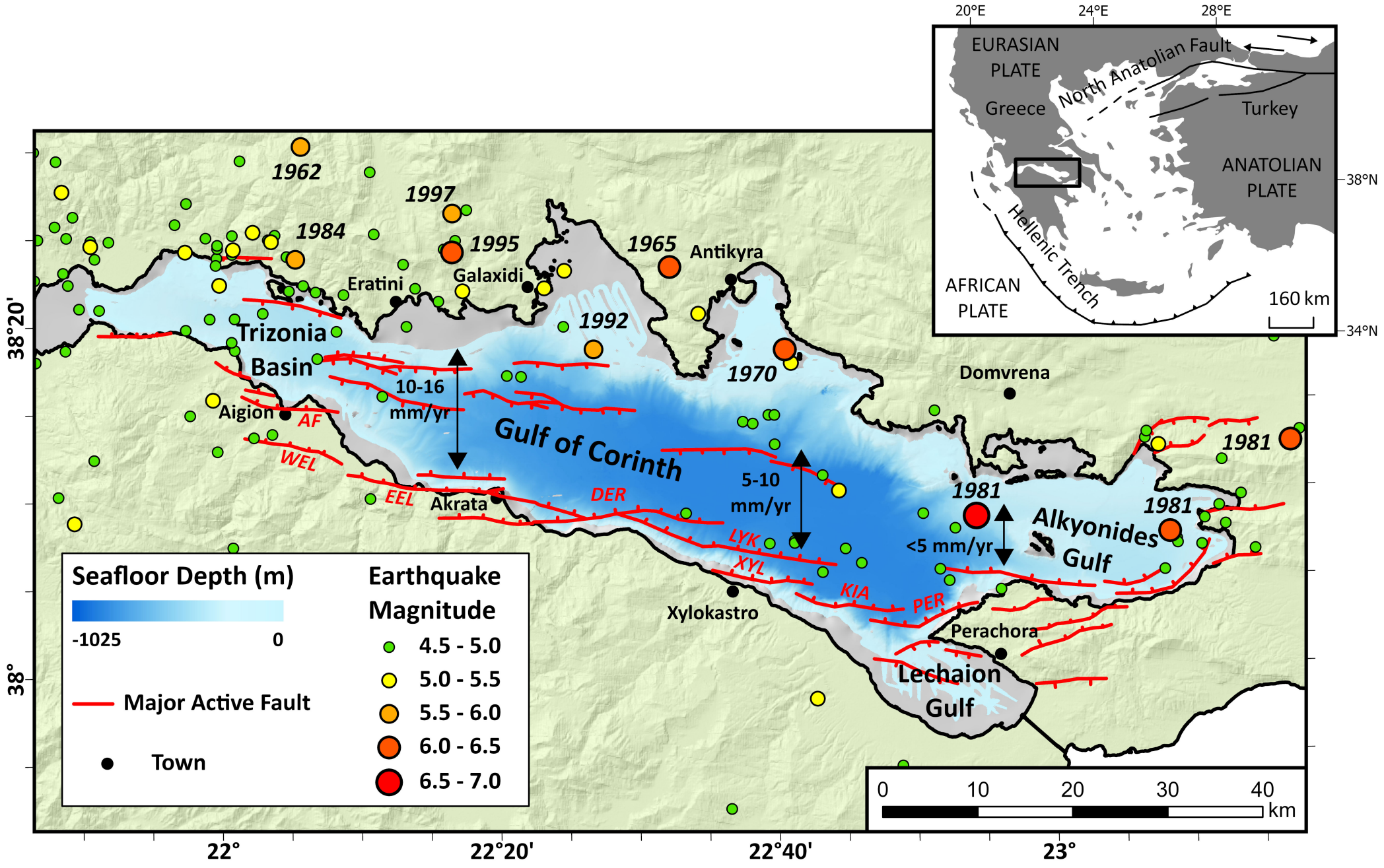
20°E
24°E
28°E
EURASIAN PLATE
North Anatolian Fault
Greece
Turkey
ANATOLIAN PLATE
38°N
Hellenic Trench
AFRICAN PLATE
160 km
34°N
38°20'
38°
1962
1997
1984
1995
1965
Antikyra
Eratini
Galaxidi
1992
Trizonia Basin
1970
Domvrena
10-16 mm/yr
Aigion
AF
WEL
EEL
Akrata
Gulf of Corinth
DER
5-10 mm/yr
1981
1981
1981
<5 mm/yr
Alkyonides Gulf
LYK
XYL
KIA
PER
Xylokastro
Perachora
Lechaion Gulf
Seafloor Depth (m)
-1025
0
Major Active Fault
Town
Earthquake Magnitude
4.5 - 5.0
5.0 - 5.5
5.5 - 6.0
6.0 - 6.5
6.5 - 7.0
0
10
20
30
40
km
22°
22°20'
22°40'
23°

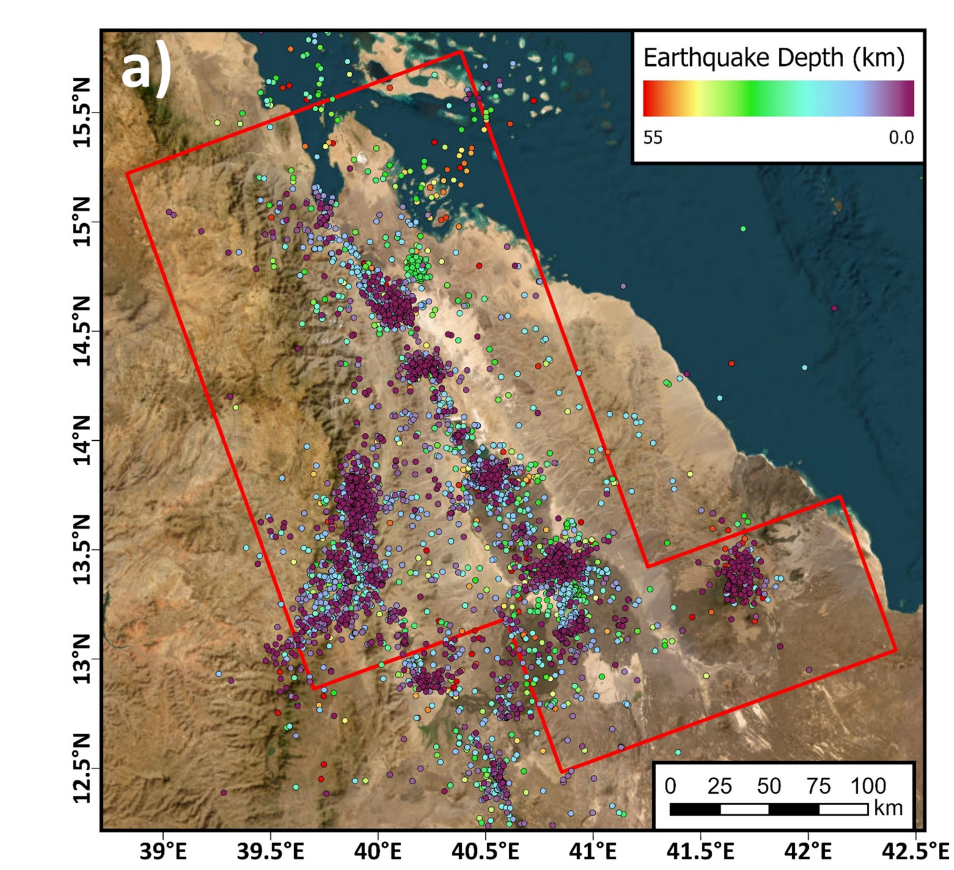
a)
Earthquake Depth (km)
55
0.0
0 25 50 75 100
km
15.5°N
15°N
14.5°N
14°N
13.5°N
13°N
12.5°N
39°E
39.5°E
40°E
40.5°E
41°E
41.5°E
42°E
42.5°E

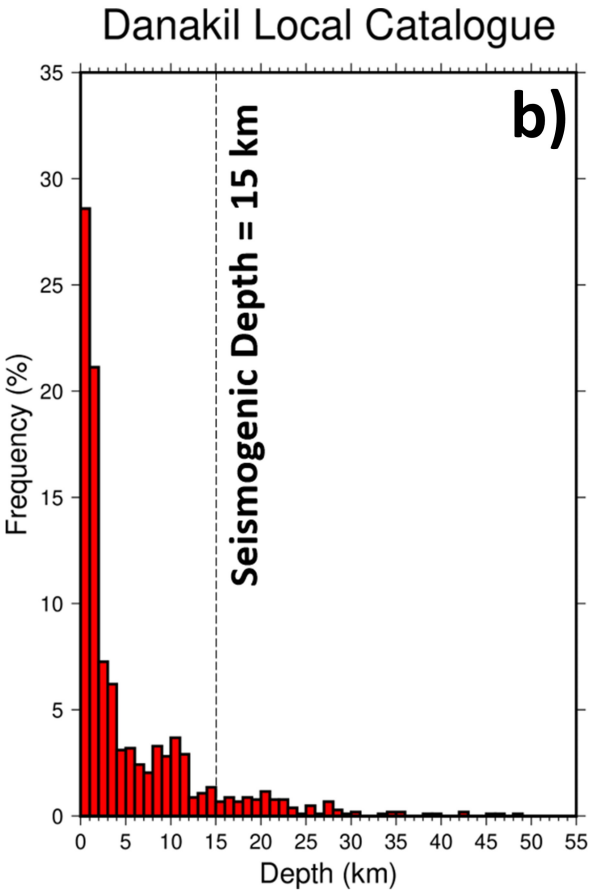
Danakil Local Catalogue
b)
Seismogenic Depth = 15 km
Frequency (%)
Depth (km)

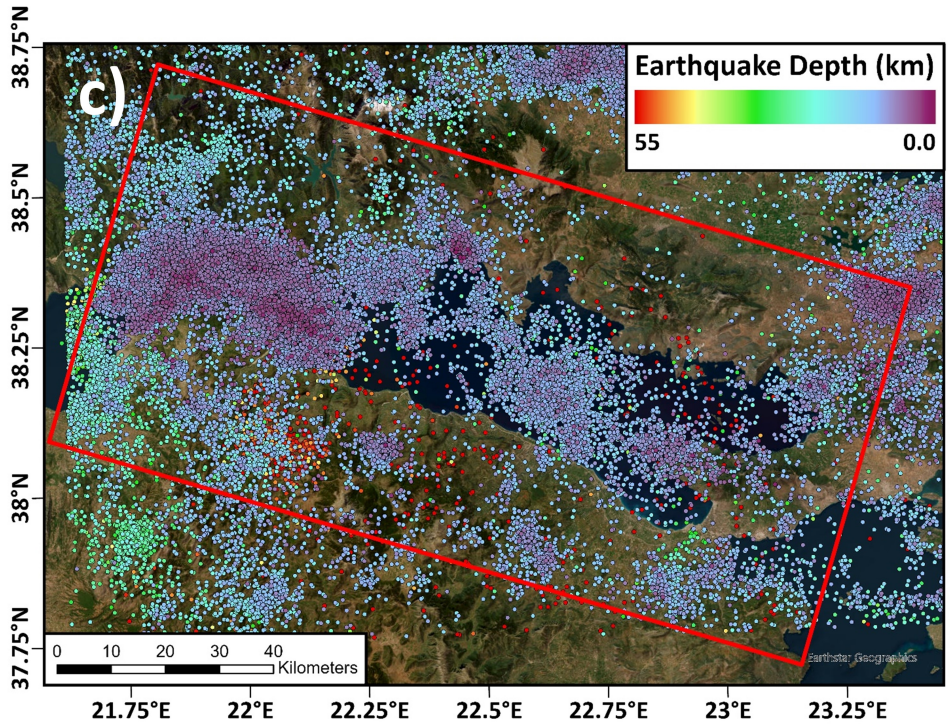
c)
Earthquake Depth (km)
55
0.0
0 10 20 30 40
Kilometers
38.75°N
38.5°N
38.25°N
38°N
37.75°N
21.75°E
22°E
22.25°E
22.5°E
22.75°E
23°E
23.25°E

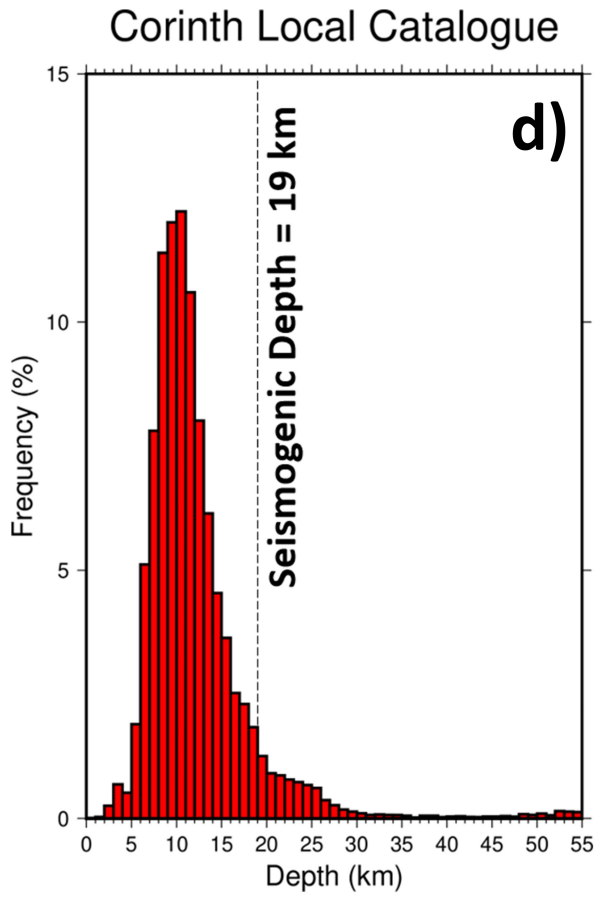
Corinth Local Catalogue
d)
Seismogenic Depth = 19 km
Frequency (%)
Depth (km)

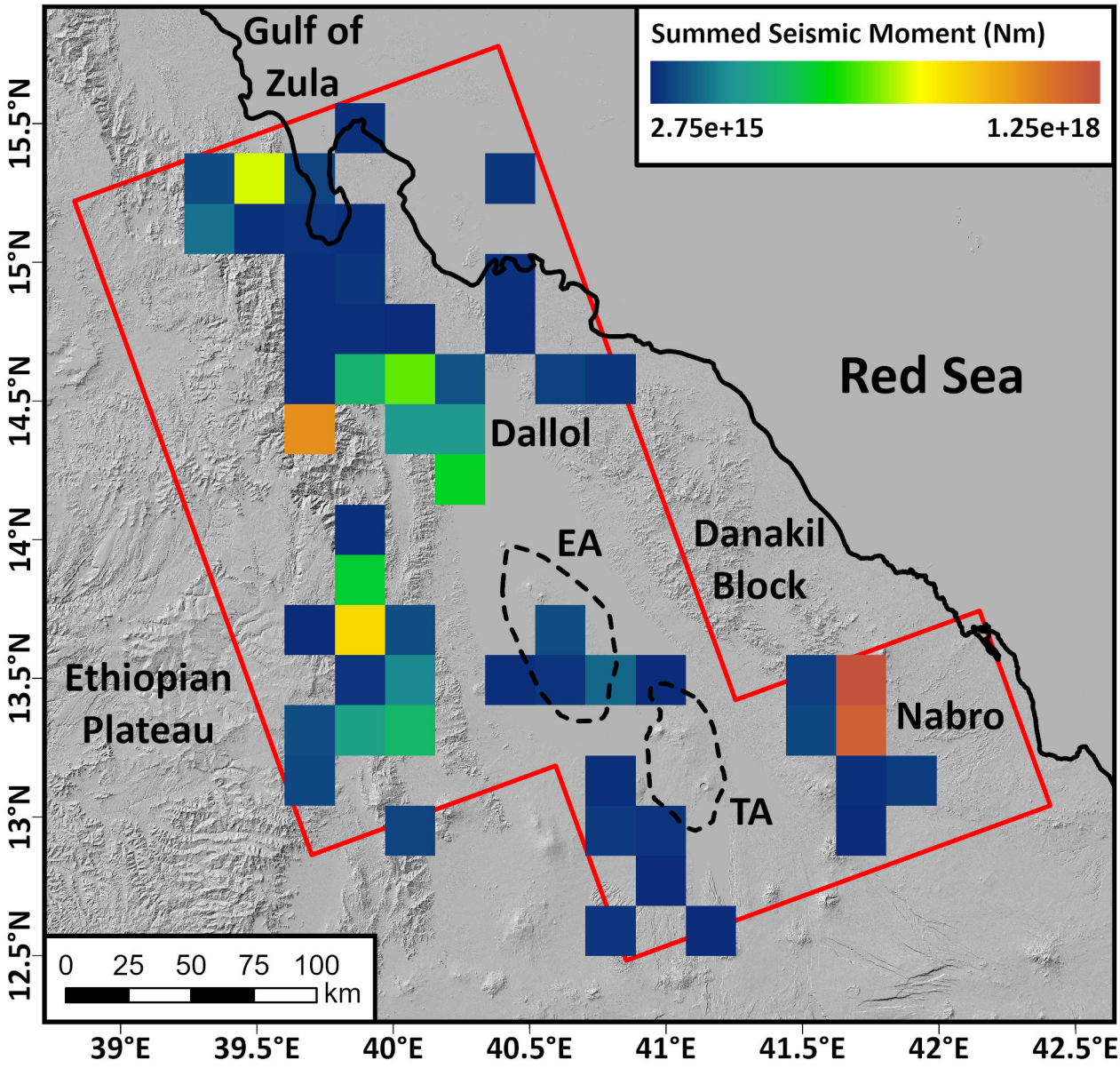
Gulf of Zula
Red Sea
Dallol
EA
Danakil Block
Ethiopian Plateau
Nabro
TA
Summed Seismic Moment (Nm)
2.75e+15
1.25e+18
0 25 50 75 100
km
15.5°N
15°N
14.5°N
14°N
13.5°N
13°N
12.5°N
39°E
39.5°E
40°E
40.5°E
41°E
41.5°E
42°E
42.5°E

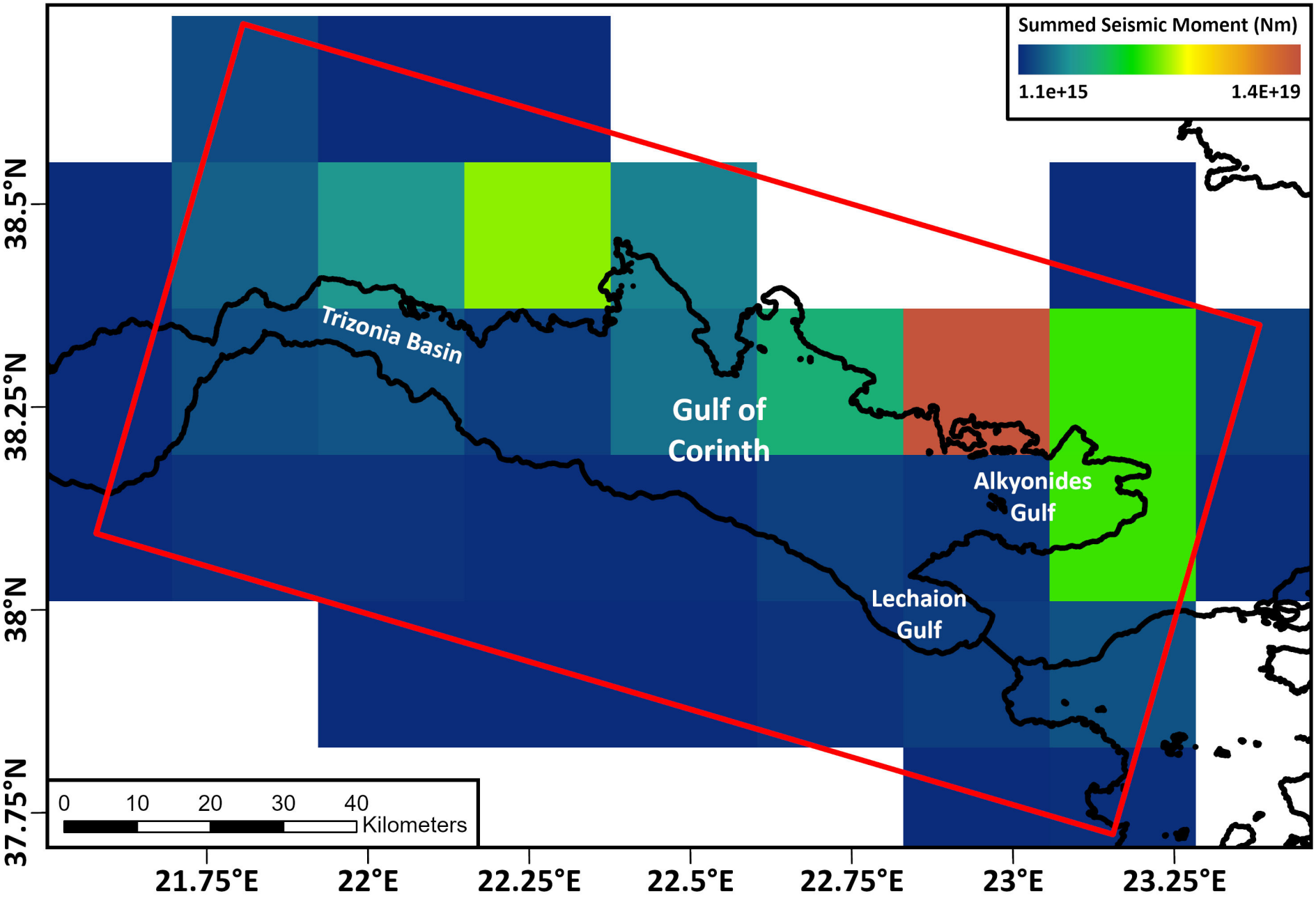
Summed Seismic Moment (Nm)
1.1e+15
1.4E+19
Trizonia Basin
Gulf of Corinth
Alkyonides Gulf
Lechaion Gulf
0 10 20 30 40
Kilometers
38.5°N
38.25°N
38°N
37.75°N
21.75°E
22°E
22.25°E
22.5°E
22.75°E
23°E
23.25°E

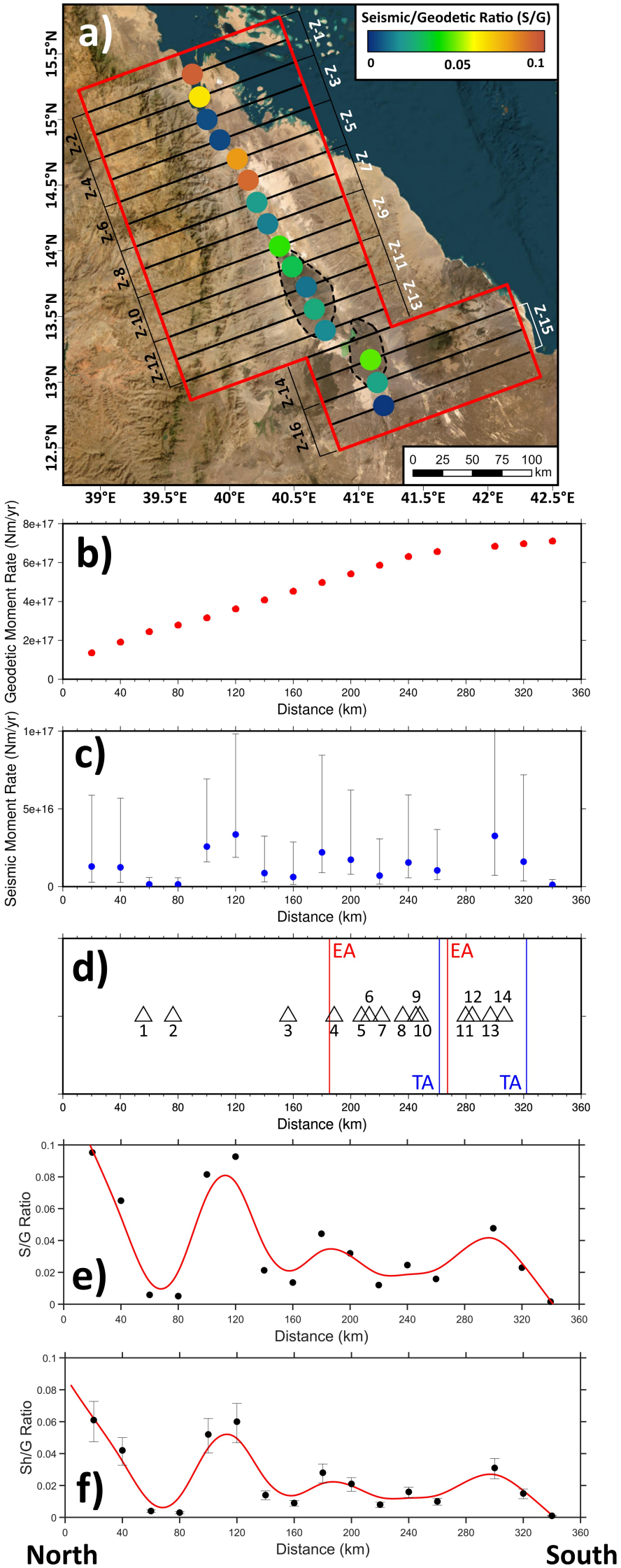
a)
Seismic/Geodetic Ratio (S/G)
0
0.05
0.1
Z-1
Z-3
Z-5
Z-7
Z-9
Z-11
Z-13
Z-15
Z-2
Z-4
Z-6
Z-8
Z-10
Z-12
Z-14
Z-16
0 25 50 75 100
km
15.5°N
15°N
14.5°N
14°N
13.5°N
13°N
12.5°N
39°E
39.5°E
40°E
40.5°E
41°E
41.5°E
42°E
42.5°E
b)
Geodetic Moment Rate (Nm/yr)
8e+17
6e+17
4e+17
2e+17
0
Distance (km)
c)
Seismic Moment Rate (Nm/yr)
1e+17
5e+16
0
Distance (km)
d)
EA
EA
1 2 3 4 5 6 7 8 9 10 11 12 13 14
TA
TA
Distance (km)
e)
S/G Ratio
0.1
0.08
0.06
0.04
0.02
0
Distance (km)
f)
Sh/G Ratio
0.1
0.08
0.06
0.04
0.02
0
Distance (km)
North
South

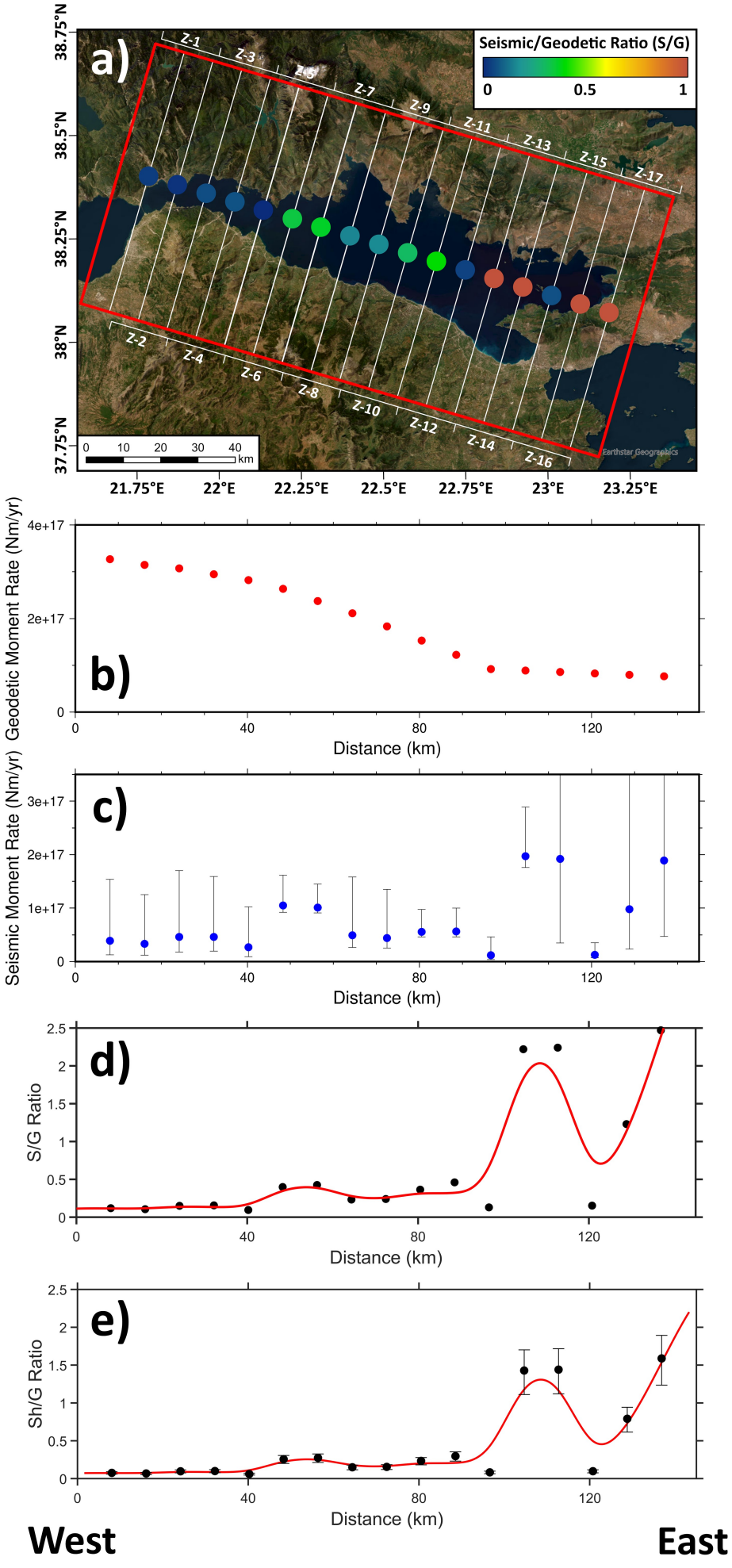
a)
Seismic/Geodetic Ratio (S/G)
0
0.5
1
Z-1
Z-3
Z-5
Z-7
Z-9
Z-11
Z-13
Z-15
Z-17
Z-2
Z-4
Z-6
Z-8
Z-10
Z-12
Z-14
Z-16
0 10 20 30 40 km
38.75°N
38.5°N
38.25°N
38°N
37.75°N
21.75°E
22°E
22.25°E
22.5°E
22.75°E
23°E
23.25°E
b)
Geodetic Moment Rate (Nm/yr)
4e+17
2e+17
0
0
40
80
120
Distance (km)
c)
Seismic Moment Rate (Nm/yr)
3e+17
2e+17
1e+17
0
0
40
80
120
Distance (km)
d)
S/G Ratio
2.5
2
1.5
1
0.5
0
0
40
80
120
Distance (km)
e)
Sh/G Ratio
2.5
2
1.5
1
0.5
0
0
40
80
120
Distance (km)
West
East